Regional Studies in Marine Science 56 (2022) 102680

Contents lists available at ScienceDirect

Regional Studies in Marine Science

journal homepage: www.elsevier.com/locate/rsma

Chlorophyll-a concentrations in the Arabian Gulf waters of arid region: A case study from the northern coast of Qatar

Sankaran Rajendran *, Noora Al-Naimi, Jassim A. Al Khayat, Caesar Flonasca Sorino, Fadhil N. Sadooni, Hamad Al Saad Al Kuwari

Environmental Science Center, Qatar University, P.O. Box: 2713, Doha, Qatar

ARTICLE INFO

Article history:
Received 1 May 2022
Received in revised form 19 September 2022
Accepted 21 September 2022
Available online 25 September 2022

Keywords:
Chlorophyll-a
Hyperion
Sentinel-2
Landsat-8
Algorithms
Qatar
Arabian Gulf

ABSTRACT

Remote sensing of spectrally active Chlorophyll-a (Chl-a) in the gulf water of an arid region is important to understand the spatial and temporal variations of phytoplankton and biomass in the water. This study characterizes the spectral absorption of Chl-a and detects and maps the Chl-a of Al Arish–Al Ghariyah coastal region of northern Qatar using the data of Hyperion of EO-1, MultiSpectral Instrument (MSI) of Sentinel-2, and Operational Land Imager (OLI) of Landsat-8 satellites. The study of image spectra of Chl-a of coastal water of the Al Ghariyah region using the Hyperion image showed spectral band absorptions near 450 and 475 nm in the blue region and around 640, 730, 760, and 830 nm in the red region. The analysis of Hyperion data using image spectra by linear spectral unmixing (LSU) method showed the occurrence of Chl-a in very shallow and shallow water. The mapping of Chl-a of the Al Arish–Al Ghariyah coastal region was carried out using MSI and OLI data by NDCI, 2BDA, 3BDA, and FLH violet algorithms, which showed the concentrations and distributions of the Chl-a in the region. The performance of the algorithms was studied using WorldView-3 data, which provided the R^2 values of 60% and the best suitability of the NDCI algorithm and MSI data to map the concentration of Chl-a. All the results were validated using field measurements, in-situ measurements, and laboratory analyses of field samples. The measurements of Chl-a showed the occurrence of poor occurrence of Chl-a and confirmed the imagery results. The remote sensing results with physical and chemical parameters of water samples allowed us to assess Chl-a concentrations in the region. This study evaluates the sensor's capability and applications of satellite data and algorithms to map concentrations of Chl-a in the Gulf waters of the arid region.

1. Introduction

Chlorophyll-a (Chl-a) is a significant contributor to primary production in the estuarine, gulf, and coastal waters of marine ecosystems worldwide (Lu et al., 2021; Salem et al., 2017; Beck et al., 2016). The concentration of Chl-a is an indicator of the abundance of phytoplankton (Cherif et al., 2021; Sosa-Ávalos et al., 2021). The phytoplankton converts CO_2 and H_2O to O_2 through photosynthesis and is responsible for primary production in the water column (Ansper and Alikas, 2019; Matthews, 2011). The literature review shows that concentrations of very high levels of Chl-a indicate poor water quality and that the long-term existence of elevated levels is a problem for the primary production of biomass (Gao et al., 2022; Ismail et al., 2020; Li et al., 2017). In general, concentrations of higher Chl-a are common during summer, when water temperatures and light levels are relatively high when compared to the winter (Li et al., 2017). The strong tidal mixing in the coastal region lowers Chl-a concentration due to the residence time of algae in the photic zone (Sala et al., 2022, 2018). Also, the tidal causes mixing of fine sediment and elevates turbidity levels, which reduces the amount of light available for photosynthesis when compared to the slow-moving waters that increase nutrients and cell numbers to grow (Tang et al., 2020). Chl-a concentrations are low in deltas, estuaries, and tidal creeks due to tidal flushing when compared with enclosed bays and shallow coastal lagoons (Stumpner et al., 2020; Seim et al., 2006). Madhupratap et al. (1996) studied winter cooling in the northeastern Arabian Sea and discussed the mechanisms of biological response. On the other hand, Shah et al. (2019) and Luis and Kawamura (2004) studied the factors such as upwelling and downwelling phenomena in the south-west coast of India and stated that the upwelling and downwelling along the west coast of India determine the major part of biological production including the fishery production over the eastern Arabian Sea. Shafeeque et al. (2019) stated that the South Eastern Arabian Sea (SEAS) region is dominated by upwelling and the seasonally-reversing winds and currents are the major physical

* Corresponding author.
E-mail address: srajendran@qu.edu.qa (S. Rajendran).

https://doi.org/10.1016/j.rsma.2022.102680

forces driving primary production. The region is characterized by high primary productivity during the summer monsoon season (June to September), when the winds and currents favor upwelling. They described the increase in chlorophyll concentration is due to the input of nutrients from terrestrial sources to coastal water. However, studies show that concentrations of Chl-a have a patchy spatial distribution and are measured vertically in the water column. Zhang et al. (2004) recorded high values of Chl-a content and primary productivity that decreased from inner to outer in the Meiliang Bay of Taihu Lake. They studied primary productivity in a vertical profile and described the maximum primary productivity that was recorded at 20–50 cm water depth in spring, summer and autumn. They stated that there was no remarkable difference in winter and that productivity was exponentially increased with water temperature from 10 to 30 degrees C. The in-situ measurement of Chl-a is challenging when the occurrences and distributions vary in time and space and is difficult to do sampling due to limited accessibility (Buma and Lee, 2020; Boucher et al., 2018; George, 2014). In the absence of continuous ground observational datasets, the advantages and potential application of satellite datasets help more to study the Chl-a concentration globally (Xu et al., 2022; He et al., 2021; Hu et al., 2021; Wang et al., 2021; Cordero-Bailey et al., 2021; Hao et al., 2019; Ansper and Alikas, 2019). In particular, the European Space Agency (ESA) climate change initiative (CCI) program realizes the full potential of the long-term global Earth Observation over the past 30 years and the ocean color project of the program provides water-leaving radiance in the visible domain, derived chlorophyll and inherent optical properties by utilizing the data archives from Copernicus, ESA, NASA and NOAA (https://climate.esa.int/en/projects/ocean-colour/).

Satellite mapping of chlorophyll concentration depends mainly on the absorption and scattering of phytoplankton. The information about Chl-a concentrations is achieved by mapping them using appropriate algorithms developed based on the spectral absorption properties of phytoplankton and other materials in the water (Lins et al., 2017; Zhang et al., 2014). Several algorithms have been developed for mapping the concentrations of Chl-a in marine and coastal waters (Pahlevan et al., 2020; Abbas et al., 2019; Moses et al., 2019; Zheng and Di Giacomo, 2017). To better estimate the concentration of Chl-a, the normalized difference chlorophyll index (NDCI) (Mishra and Mishra, 2012; Shahzad et al., 2018), two and three-band algorithms (2BDA, 3BDA) (Watanabe et al., 2018; Abdelmalik, 2018; Dall'Olmo and Gitelson, 2005; Gitelson et al., 2003), fluorescence line height (FLH) (Zhao et al., 2010), and surface algal bloom Index (SABI) (Alawadi, 2010) algorithms were used. The 2BDA, 3BDA, and NDCI are considered portable algorithms to map Chl-a concentrations (Buma and Lee, 2020; Pereira Sandoval et al., 2019; Beck et al., 2016). Toming et al. (2016) presented the first results using Sentinel-2A satellite data and simple band ratio algorithms to estimate water quality parameters including the Chl-a and dissolved organic carbon in small and large lakes in Estonia. Chen et al. (2017) used band ratio algorithms to retrieve colored dissolved organic matter (CDOM) and Chl-a concentrations in Lake Huron using the data and identified the B5/B4 (2BDA) as best for the Chl-a retrieval. Also, studies were carried out using hyperspectral data namely Hyperion data (Katlane et al., 2020; Richard et al., 2018) and multispectral data such as Sentinel-2 (Pahlevan et al., 2020; Caballero et al., 2020; Ansper and Alikas, 2019), Sentinel-3 (Cherif et al., 2021; Tuuli et al., 2020), Landsat-8 (Buma and Lee, 2020; Boucher et al., 2018; Fu et al., 2018) and WorldView-2 and 3 (Buma and Lee, 2020; Wang et al., 2018). The performance of these algorithms for the estimation of Chl-a concentration using Sentinel-2 and Landsat-8 data has been evaluated based on a very high-resolution WorldView satellite dataset by Buma and Lee (2020) and Beck et al. (2016). Xu et al. (2019) stated that Sentinel-2A multispectral optical sensor senses signal of the water column up to about 1.5 m deep from the water surface in Harsha Lake and there is no light scattering back out of water beyond the depth and the data can be well utilized to map the Chl-a concentration of the Lake. They compared the satellite data results with in-situ measurements of Chl-a measured at the depth of 0.3–0.5 m using a YSI sonde (Yellow Springs Instrument, Inc.). Buma and Lee (2020) stated that a future study combining the data products provided by Sentinel-2 and Landsat-8 may be appropriate for water quality estimation and could create a more reliable means for quantifying Chl-a.

In this context, hyperspectral remote sensing is used for mapping, classification, and monitoring estuarine areas and coastal ecosystems. The technique is capable of assessing water quality (Joydas et al., 2015), and mapping the concentration of Chl-a (Katlane et al., 2020; Beck et al., 2016). A literature review shows that Chl-a exhibits strong absorption in blue and red regions, and high reflectance in green and near-infrared (NIR) regions (Kirk, 1994). Three important features of Chl-a were identified to study the concentration of Chl-a viz. (1) strong absorptions around 670 nm (which also depends on the concentration of inorganic and organic suspended solids, Yacobi et al., 1995) and (2) a peak near 685 nm in the red region due to Chl-a fluorescence (Doerffer, 1981; Gower, 1980), and (3) a peak in the NIR region around 700 nm (Gernez et al., 2017). Also, studies show the absorption of Chl-a in the blue region between 440 and 475 nm and a high reflectance near 500 nm in the green region (Grendaitė et al., 2018; Solonenko and Mobley, 2015). The feature that occurred near 700 nm is mostly well utilized to develop algorithms and map Chl-a concentrations (Tuuli et al., 2020; Beck et al., 2016). Recently, Katlane et al. (2020) studied the Hyperion data and developed a ratio using the blue and green bands as Chl-a = 0.005 x (Band11:457 nm/Band18:528 nm) and showed the spatial distribution of Chl-a of Kneiss archipelago Gul, Gabes, Tunisia. Also, Gernez et al. (2017) studied the reflectance spectra ($\rho w\lambda$) that were measured at 400–900 nm in the Bourgneuf Bay (French Atlantic coast) using TriOS radiometers. They showed the presence of significant absorptions between 600 and 900 nm (Fig. 1a in Supplementary material). They stated that the presence of significant deep and broad absorptions around 675 nm (dotted red rectangle, Fig. 1a in Supplementary material) and reflectance around 700 nm (dotted green rectangle, Fig. 1a in Supplementary material) are attributed to the presence of Chl-a (Gernez et al., 2017; Méléder et al., 2005). The slope between 675 to 700 nm is referred to as the NIR/red edge (Gons et al., 2002). The spectra measured do not show any absorption of Chl-a between 400 and 580 nm. Thus, the spectral bands of multispectral sensors of Sentinel-2 and 3, Landsat-8, etc. can be studied with the unique spectral absorptions of Chl-a to map the concentrations of Chl-a in a lake and coastal water (Table 1 and Fig. 1b in Supplementary material).

However, much effort has been taken to estimate the concentration of Chl-a in the gulf water of the arid region, especially around Qatar. A literature review shows that Al-Naimi et al. (2017) used a set of in-situ Chlorophyll-a measurements collected from 24 locations in the central Arabian Gulf, and evaluated the performance of the Visible Infrared Imaging Radiometer Suite (VIIRS) for the first time to map Chl-a of the region. They stated that remotely sensed Chl-a observations are adequate in seasonal cycles and that a regional-tuned algorithm is needed to provide a better estimation of the surface Chl-a of the region. Recently, Rakib et al. (2021) studied the variability of physical and biogeochemical parameters of the central Arabian Gulf from in-situ measurements. They stated that the Chl-a is relatively high during late summer in the offshore region, while it is very low in the

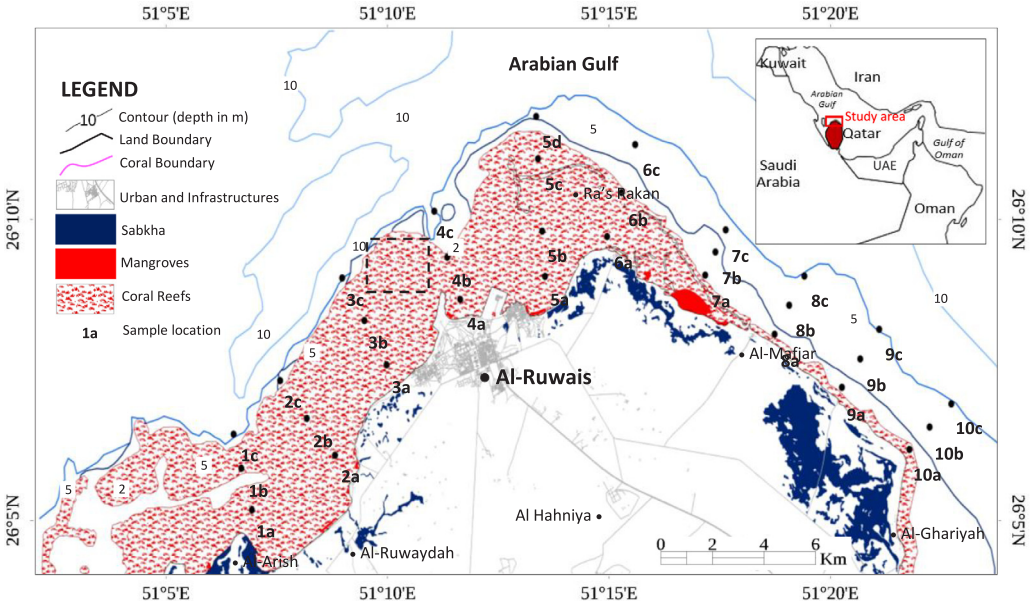

Fig. 1. Study area, showing the occurrence and distribution of mangroves, sabkhas, and coral reefs along the coastal region between the Al Arish and Al Ghariyah, the northern part of the State of Qatar. The dashed rectangle is the area chosen to evaluate the algorithms.

nearshore region, which is linked to anthropogenic stresses from the central east coast of Qatar. Hussein et al. (2021) discussed the spatiotemporal variability of Chl-a and Sea Surface Temperature (SST) and their relationship with bathymetry over the coasts of UAE. They utilized the MODIS Aqua data from 2003 to 2019 and stated that the highest concentrations of Chl-a were seen in the Strait of Hormuz with an average of 2.8 mg m^{-3} which is 1.1 mg m^{-3} higher than the average for the entire study area. They stated that the fluctuation of Chl-a levels over time is to be monitored regularly and that the concentration of Chl-a is to be studied in the Gulf water of the arid region to understand the phytoplankton abundances and primary production of the Gulf water. Therefore, this study aims to map the concentrations of Chl-a in the Al Arish–Al Ghariyah coastal region of Qatar, which has a very shallow depth and significant anthropogenic activities in the Arabian Gulf (Fig. 1). The objectives of the study are to describe the spectral band absorptions of Chl-a, to detect the Chl-a occurrence using hyperspectral Hyperion data of EO-1, to map the concentration of Chl-a using the data of MSI of Sentinel-2 and OLI of Landsat-8 satellites by NDCI, 2BDA, 3BDA, and FLH violet algorithms and to assess the concentration using the data collected by in-situ measurements. This study analyzes the performance of algorithms using high spatial resolution WorldView-3 data and demonstrates the suitability of satellite data and the most appropriate algorithms to map the Chl-a concentrations of the Al Arish–Al Ghariyah coastal region of Qatar to recommend them to a similar region of the world.

2. Study area

The State of Qatar is positioned between 24°N and 30°N latitude and 48°E and 57°E longitude along the east coast of the Arabian Gulf. The study area between Al Arish and Al Ghariyah coastal regions has a gentle slope of bathymetry and low topographic elevations (Fig. 1) (Purkis and Riegl, 2012), and is situated in a desert climate having a very mild winters and in a very hot and sunny summers arid environment. December to March (winter) and June to September (summer) are the two transition periods (Al Senafi and Anis, 2015), and temperatures up to 51 °C during summer and 15 °C during winter are observed (Sheppard, 1993). During summer, the coastal water around the region is hottest and the sea surface temperature exceeds 30 °C in August. The humidity varies between the seasons and ranges from 21 to 55% during summer and winter, respectively (Al Senafi and Anis, 2015). The northwesterly "shamal" wind strongly influences coastal currents and storm surges (Cavalcante et al., 2016). The region has high evaporation rates, causing extreme salinity with an average of 42 ppt, and increasing to > 70 ppt in lagoons (John et al., 1990). The high evaporation rates in low-lying intertidal areas develop coastal salt flats (sabkha) along the coast (Cavalcante et al., 2016). The coastal region has salt marshes, mudflats, and mangrove forests, and the algal beds, seagrass meadows, and coral reefs occur in the subtidal areas (Fig. 1) (Vaughan and Burt, 2016; Burt, 2014). The coastline exposes well to the occurrence of carbonate platforms and shelf edges. The gentle bathymetry is deposited by clay, mud, and sand sediments which support the growth of mangroves, seagrasses, plants, and microbials (Lokier and Fiorini, 2016; Lokier et al., 2013). These support higher biodiversity and productivity and the region acts as a natural laboratory for studying the various marine ecosystems, particularly the environment of coral reefs (Vaughan and Burt, 2016; Burt, 2014; Purkis and Riegl, 2012). A study using satellite imagery and LiDAR (light detection and ranging) based bathymetry shows that the region has linear shoal bodies extending seaward to 4 to 5 m depth. The study of Chl-a concentrations in the Al Arish and Al Ghariyah coastal regions, is an analog for similar regions of the world.

3. Materials and methods

3.1. Satellite data and mapping methods of Chl-a

In this study, the spectral band absorption and detection of Chl-a in the Al Ghariyah region were carried out using Hyperion data by the linear spectral unmixing method (LSU). The mapping of Chl-a was carried out using the data of MSI (MultiSpectral Instrument) of Sentinel-2 and OLI (Operational Land Imager) of Landsat-8 by applying normalized difference chlorophyll index (NDCI), two-band (2BDA), and three-band (3BDA) algorithms and fluorescence line height (FLH) violet algorithm to understand the occurrence and concentration of Chl-a in the region.

3.1.1. Satellite data and pre-processing

i. Hyperion data: The Hyperion sensor of the EO-1 satellite provides 242 spectral bands at a bandwidth of ∼10 nm in the spectral region of 400–2500 nm. The sensor covers a spatial extent of 7.5 km in width and 105 km in length with a spatial resolution of 30 m. The system has two grating spectrometers; one visible/near-infrared (VNIR) spectrometer (approximately 0.4–1.0 μm) and one short-wave infrared (SWIR) spectrometer (approximately 0.9–2.5 μm). The signal-to-noise ratio (SNR) for the VNIR detector is from ∼140:1 to 190:1, and for the SWIR detector is from 96:1 to 38:1 (Pearlman et al., 2003). In this study, we acquired data dated July 16, 2010, that was available near the Al Ghariyah region to show the Chl-a of the region. The pre-processing of data including the rescaling of radiance, removal of spectrally overlapping bands and bad bands, de-striping, smile effect correction, geometric rectification, and an atmospheric correction were carried out using ENVI image processing software (Goodenough et al., 2003) (ENVI 5.5, https://www.harrisgeospatial.com). During which, the bands that had no spectral information (1–9, 58–81, 120–128, 165–174, and 225–242 bands) were removed and a total of 168 bands (45 in VNIR and 123 in SWIR) were used in this study. The Hyperion Level 1R product was not geometrically corrected and therefore the data were georeferenced using Ground Control Points (GCPs) through the selection of 17 points and first-order transformation with an overall root-mean-square error (RMSE) of 0.01312. The scattering of molecular and particulates, absorption at the radiance-at sensor, and retrieval of the values of the reflectance at the surface were carried out using the Fast Line-of-sight Atmospheric Analysis of Spectral Hypercubes (FLAASH) tool available in the software (Anderson et al., 2002; Rajendran et al., 2021). The spectral band absorptions of Chl-a were studied and the pixels representing the Chl-a in the very shallow, shallow, and deep waters of the coastal region were detected by the linear spectral unmixing method (Abuzied et al., 2016).

ii. Sentinel-2 MSI data: The Sentinel-2 mission consists of two polar-orbiting satellites, viz., the Sentinel-2A and 2B, launched on 23 June 2015 and 7 March 2017, respectively, in a sun-synchronous orbit at 786 km altitude with an inclination of 98.62° phased at 180° to each other. Each satellite carries a MultiSpectral Instrument (MSI) having a swath width of approximately 290 km and 13 spectral bands in the visible, red-edge, near-infrared, and shortwave infrared regions (430 nm to 2320 nm) with spatial resolutions of 10 m, 20 m, and 60 m, and radiometric resolution of 12-bit. The satellites have a revisit time of 10 days with one satellite and 5 days with two satellites at the equator (Drusch et al., 2012). Although the mission was designed for land applications, its imaging capabilities allowed the remote sensing community to study coastal and inland water monitoring (Ruddick et al., 2016). Scientists started to utilize the data as a suitable solution for coastal research mapping (Tuuli et al., 2020; Mohamed et al., 2019; ESA, 2015). Importantly, bands 4, 5, and 6 (665, 705, and 740 nm respectively) of MSI have a relatively narrow bandwidth that corresponds to the spectral region's sensitivity of the Chl-a pigment (Ansper and Alikas, 2019; Liu et al., 2017). To map the Chl-a of the Al Arish–Al Ghariyah region, we downloaded the free data of December 15, 2020, the day closer to the day of fieldwork, from the Sentinel's Scientific Data Hub and used. The collected MSI Level-1C data was preprocessed using the Sentinel Application Platform (SNAP) program, which has the Sen2Cor plugin and Sentinel-2 Toolbox (http://step.esa.int/main/toolboxes/snap/) (Louis et al., 2016; Clevers and Gitelson, 2013). The data were projected to the UTM Zone 39N projection with reference to the WGS 1984 ellipsoid. Since the spatial resolutions vary for the different spectral bands, 20 m resampling was performed using the Resampling tool (v2.0) to do Chl-a mapping. The identification of cloud-free pixels was carried out using IdePix (v2.2).

iii. Landsat-8 OLI data: Landsat-8 (NASA's satellite launched in February 2013) produces 11 spectral bands, by two sensors, namely the Operational Land Imager (OLI) and the Thermal Infrared Sensor (TIRS). The OLI sensor consists of nine bands with a spatial resolution of 30 m for bands 1 to 7 and 9. The bands 1 (433–453 nm) and 9 (1360–1390 nm) are useful for coastal aerosol studies and cirrus cloud detection. The spatial resolution of band 8 (panchromatic) is 15 m. The TIR sensor collects the thermal bands 10 and 11 at 100 m spatial resolution. The approximate size of the scene is 170 km north–south by 183 km east–west. The OLI has narrower bandwidths in the red, near-infrared (NIR), and shortwave infrared (SWIR) bands when compared with the sensors of the previous Landsat missions. The Landsat-8 has an increased signal-to-noise ratio (SNR) and a radiometric resolution of 16 bits. Though the sensors are built for terrestrial applications, these bands have proven useful for mapping Chl-a in water bodies (Pahlevan et al., 2014). Therefore, in this study, the Level-1 terrain-corrected (L1T) data of December 17, 2020, was downloaded from the US Geological Survey (http://earthexplorer.usgs.gov) and used to study the Chl- of the study region. The data have been radiometrically and geometrically corrected and projected to the UTM Zone 39N projection and WGS 1984 ellipsoid, similar to the Sentinel-2 data. The preprocessing of data was carried out using QGIS open-source software.

iv. WorldView-3 data: The WorldView-3 (WV3) satellite is operating at an altitude of 617 km and has an average revisit time of <1 day. The sensor produces a very high spatial resolution panchromatic (450–800 nm) image at 0.31 m, eight multispectral visible infrared (VNIR) images viz. red, red edge, coastal, blue, green, yellow, near-IR1, and near-IR2 (400–1040 nm) at 1.24 m, and eight short wave infrared (SWIR) images at 3.7 m. In this study, the data consisting of eight multispectral bands acquired on June 29, 2019, were purchased from https://www.digitalglobe.com and used in an area of interest. The data were georeferenced to the UTM zone 39N projection using the WGS84 datum and carried out for geometric, radiometric, and atmospheric corrections using ENVI image processing software. Tables 1 and 2 in the Supplementary material provide details about the sensor characters of MSI and OLI and the data that were used in this study respectively.

3.2. Detection and mapping of Chl-a

Initially, we studied the spectral absorption of Chl-a that is present in very shallow, shallow, and deep waters of the coastal region using the image spectra of Hyperion data. Then, the detection of Chl-a in the water was carried out using the data obtained by the LSU method (Abuzied et al., 2016). The method determines the abundance of Chl-a that can be depicted in imagery based on the spectral characters. Here, the reflectance at each pixel of the image is assumed as a linear combination of the reflectance of each material (or end member) that is present within the pixel (Abuzied et al., 2016). Further, the mapping of Chl-a was carried out using MSI and OLI data and image processing algorithms. In this study, we used the NDCI, FLH violet, 2BDA, and 3BDA ratios algorithms over the satellite data and studied the Chl-a concentrations in the water of the Al Arish–Al Ghariyah coastal region (Table 3 in Supplementary material). This study assesses the performance of algorithms using high spatial resolution WV3 data and field knowledge (Watanabe et al., 2018; Liu et al., 2017; Beck et al., 2016). Beck et al. (2016) studied the Chl-a of Harsha Lake which is situated in southwest Ohio using several algorithms with the data of Compact Airborne Spectrographic Imager (CASI), Medium Resolution Imaging Spectrometer (MERIS), WorldView-2, Sentinel-2, Landsat-8, and Moderate Resolution Imaging Spectrometer (MODIS). They stated that the NDCI algorithm performed better than the CI (Cyanobacterial Index), FLH,

Table 1
Results of Pearson's test linear regression performed using different algorithms and MSI and OLI data for mapping of Chl-a of the Al Arish-Al Ghariyah region.

Sensors	Algorithms	Pearson's R	Pearson's R^2	p-value	Slope	Intercept
MSI of Sentinel-2 (20 m)	NDCI	0.775	0.601	<0.001	0.864	−0.308
	2BDA	0.769	0.592	<0.001	0.549	−0.020
	3BDA	0.648	0.420	<0.001	0.012	−0.430
	FLH-violet	0.692	0.478	<0.001	0.445	−0.033
OLI of Landsat-8 (30 m)	NDCI	0.251	0.063	<0.001	0.138	−0.102
	2BDA	0.604	0.364	<0.001	−0.10	0.035
	3BDA	0.252	0.063	<0.001	−0.004	−0.069
	FLH-violet	0.697	0.486	<0.001	0.398	−0.024

Table 2
Results of the in-situ measurements of temperature (T), electrical conductivity (Ec), hydrogen ion concentration (pH), total dissolved solids (TDS) and Chlorophyll-a (Chl-a) in the coastal surface water between Al Arish–Al Ghariyah region of northern Qatar.

Sample No	Latitude	Longitude	T (C°)	Ec (μS/cm)	pH	TDS (g/L)	Chl-a, (μg/L)
la	26°5′11.04″N	51°7′2.59″E	26.236	58 296	8.16	37 027	0.52
lb	26°5′52.01″N	51°6′48.25″E	25.62	70 941	8.08	36 651	0.43
1c	26°6′25.40″N	51°6′37.82″E	21.7	52 055	8.04	36 110	0
2a	26°6′4.90″N	51°8′54.07″E	28.515	63 684	8.2	38 795	0.32
2b	26°6′40.97″N	51°8′16.27″E	26.745	59 804	8.01	37 632	0.3
2c	26°7′17.96″N	51°7′40.34″E	21.17	51 368	9.8	36 014	0.02
3a	26°7′33.57″N	51°10′3.37″E	29.394	62 902	8.16	37 727	0.25
3b	26°8′17.04″N	51°9′33.62″E	28.154	60 370	8.04	37 020	0.15
3c	26°8′58.92″N	51°9′3.69″E	21.17	51 294	7.97	35 979	0.01
4a	26°8′37.91″N	51°11′42.38″E	23.27	53 634	7.86	36 037	0.35
4b	26°9′19.22″N	51°11′24.98″E	24.14	54 578	7.94	36 112	0.28
4c	26°10′4.46″N	51°11′7.47″E	20.5	50 662	7.93	36 066	0
5a	26°9′0.50″N	51°13′36.42″E	29.964	45 896	8	27 243	0.73
5b	26°9′44.84″N	51°13′32.71″E	27.57	56 627	8.05	35 092	0.25
5c	26°10′55.94″N	51°13′26.97″E	20.32	50 698	8	36 190	0.11
5d	26°11′37.49″N	51°13′24.51″E	20.66	51 181	8.02	36 275	0.07
6a	26°9′39.51″N	51°14′59.82″E	28.315	60 359	8.17	36 898	0.36
6b	26°10′22.70″N	51°15′19.32″E	27.88	58 596	8.17	36 117	0.37
6c	26°11′9.87″N	51°15′37.66″E	19	49 636	8.01	36 172	0.02
7a	26°9′1.60″N	51°17′11.72″E	20.08	50 495	8.01	36 226	0.01
7b	26°9′24.32″N	51°17′25.58″E	20.6	50 477	7.97	33 786	0.14
7c	26°9′46.08″N	51°17′39.34″E	20.4	50 562	8.02	36 038	0.02
8a	26°8′3.48″N	51°18′45.04″E	26.38	54 945	8.06	34 800	0.28
8b	26°8′32.07″N	51°19′4.70″E	21.1	50 122	8.01	25 795	0.36
8c	26°9′0.65″N	51°19′25.15″E	21.67	50 652	8.02	35 149	0.21
9a	26°7′11.40″N	51°20′15.51″E	25.653	53 713	7.92	34 478	0.12
9b	26°7′39.20″N	51°20′40.17″E	21.4	49 799	8.02	34 749	0.34
9c	26°8′8.28″N	51°21′5.62″E	21.6	49 755	8.02	34 606	0.21
10a	26°6′10.26″N	51°21′46.10″E	26.27	54 305	7.94	34 284	0.3
10b	26°6′32.36″N	51°22′13.19″E	25.624	53 289	8.09	34 218	0.15
10c	26°6′55.01″N	51°22′42.47″E	22.1	49 963	8.03	34 371	0.15

2BDA, and 3BDA algorithms, and that the outcome of the FLH algorithm using Landsat-8 data does not suppress illumination variations over scenes. In this study, the high spatial resolution (0.3 m) data of WV3 were used to develop training and validation datasets and studied with the datasets of MSI and OLI. During this study, we resampled the MSI bands 4 (10 m resolution) to match the resolutions of the bands 5 and 8b (20 m) by the nearest neighbor method, and thus the results of 2BDA, 3BDA, and NDCI algorithms were obtained in 20-m resolution while maintaining the FLH at its original 10-m resolution.

3.3. Field and laboratory studies

Field studies were carried out in the coastal region between Al Arish and Al Ghariyah regions during November and December 2020, the days closer to Sentinel-2 and Landsat-8 satellites passing over the study region. During the fieldwork, photographs were taken and surface water samples were collected at 31 sites using a Niskin water sampler (Model 1010, 5L) in the 10 transects across the coast (Fig. 2a in Supplementary material). The sites were selected at a distance of approximately 1 km from the coast to a 3 km offshore transect at 5 km intervals on the coastline using a GPS (Fig. 1). The underwater photography and samples were carried out to a maximum depth of 7 m (Fig. 2b and c in Supplementary material). Also, in-situ measurements for temperature (T), electrical conductivity (Ec), hydrogen ion concentration (pH), total dissolved solids (TDS), and Chlorophyll-a were carried out at the sites using YSI (Yellow Springs Instrument, Inc.) EXO2 Multi-Parameter water quality sonde (Fig. 2d in Supplementary material). Xu et al. (2019) stated that the Sentinel-2A multispectral optical sensor senses signals from the water column up to 1.5 m deep from the water surface in Harsha Lake. There was no light scattering back out of water beyond the depth of 1.5 m. Understanding that, we measured Chl-a concentration for each site at a depth less than 0.5 m to correlate well with the results of remotely sensed data. About 3 l of water samples were collected in plastic water bottles at each site and analyzed for major and trace element concentrations by Inductively Coupled Plasma - Optical Emission Spectrometry (ICP-OES). All the results were studied to understand the results retrieved from satellite data to understand the concentrations of Chl-a in the study region.

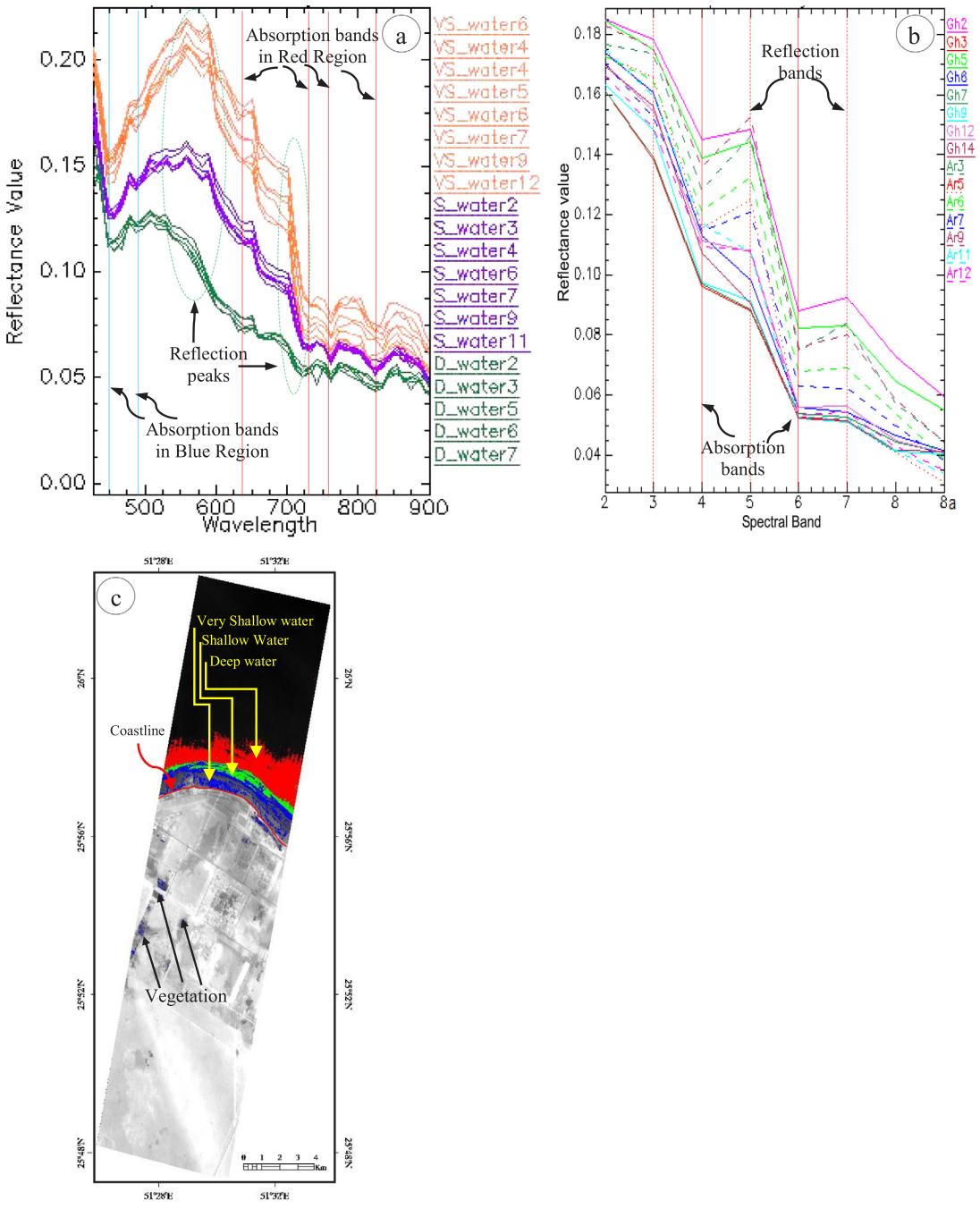

Fig. 2. Image spectra of very shallow (>1 m), shallow (1 to 2 m), and deep (<2 m) waters collected over (a) the Hyperion image of Al Ghariyah region, (b) the MSI image of Al Ghariyah and Al Arish regions (Refer Figure 2 in Supplementary material for the locations of the image spectra collection), and (c) the spatial distribution of Chl-a of Al Ghariyah region mapped using Hyperion data and by LSU method. . (For interpretation of the references to color in this figure legend, the reader is referred to the web version of this article.)

4. Results

4.1. Spectral absorptions and detection of Chl-a of study area

Image spectra of Hyperion data (Fig. 2a) were collected over the pixels representing Chl-a that were distributed in very shallow (<1 m), shallow (1–2 m), and deep (>2 m) waters near the Al-Ghariyah region based on field studies and visual interpretation of the true-color image of Sentinel-2 (see Fig. 3a in Supplementary material). The spectra of Chl-a show the presence of prominent absorptions around 450 and 475 nm in the blue region (solid blue vertical lines) and near 640, 730, 760, and 830 nm in the red region (solid red vertical lines) due to the presence of Chl-a in the algae, plants, seagrasses, etc. that occurred in the area. The presence of high reflectance near 550 nm in the green region and 700 nm in the red region (dashed green ellipticals) were observed as studied by Gitelson (1992). The spectra of very shallow depths of water (VS_water6 to VS_water12), shallow water (S_water2 to S_water11), and deep water (D_water2 to D_water7) show differences in their relative absorptions and reflectances (Fig. 2a). The spectra of very shallow water show high reflectance values when compared with the values of the shallow and deep waters. The high reflectance may be due to the reflectance energy from the water and bottom sediments

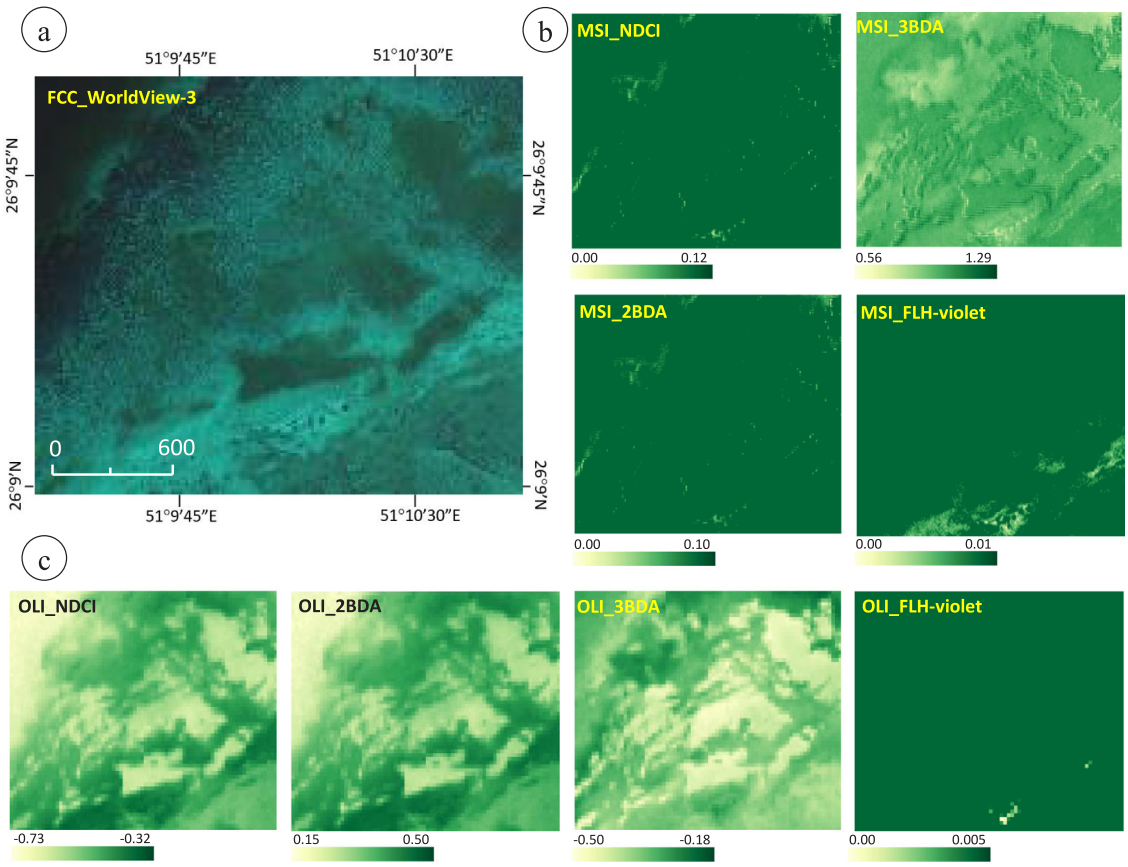

Fig. 3. Chl-a concentration in (a) WorldView-3 FCC image (R:7, G:2; B:1), (b) MSI, and (c) OLI images developed using NDCI, 2BDA, 3BDA, and FLH violet algorithms (all images are stretched into a common size). . (For interpretation of the references to color in this figure legend, the reader is referred to the web version of this article.)

that occurred at very shallow depths. The absorptions of shallow and deep waters exhibit a similar trend to very shallow water but show relatively low reflectance values, which may be due to the relatively high absorption of light by the water and the near-surface occurrence of sea plants, grasses, corals, massive sea meadows, etc. We also collected image spectra of visible and NIR bands of the MSI data for the regions near Al Ghariyah and Al Arish based on the field study (Fig. 2b, locations of image spectra are given in Fig. 3b and c in Supplementary material). The image spectra of the regions show spectral band absorptions in the MSI bands 4 and 6 (solid red vertical lines) equivalents of 665 nm and 740 nm in the red wavelength region (Table 1 in Supplementary material) and the reflections in the bands 3 (560 nm), 5 (705 nm), and 7 (786 nm) in the green and red edge regions (dashed red vertical lines, Fig. 3b). The study of the absorption and reflectance of the spectral bands of Hyperion and MSI data reveals that these bands can be well utilized to map the Chl-a of the regions. Based on this, the detection of Chl-a was carried out in the Al Ghariyah region using Hyperion data. We chose the image endmembers of very shallow, shallow, and deep waters (Fig. 2a), and mapped the Chl-a by the linear spectral unmixing (LSU) method (Rajendran et al., 2021). The result of the mapping is given in Fig. 2c. The image shows the presence of Chl-a in the very shallow (in blue), shallow (in green), and deep (in red) waters of the region clearly with their relative distributions. The results can be better interpreted and studied with MSI images and field photographs of the area (Fig. 3b–f in Supplementary material).

4.2. Chl-a mapping of MSI and OLI

4.2.1. Evaluation of algorithm

Literature review shows numerous water quality satellite reflectance algorithms have been used for retrieving Chl-a concentration where no Chl-a ground truth data is available and difficult to measure in-situ data in an area like the Al Arish–Al Ghariyah region (Watanabe et al., 2018; Richard et al., 2018; Shahzad et al., 2018). Studies show the use of NDCI (Mishra and Mishra, 2012; Shahzad et al., 2018), FLH (Zhao et al., 2010), 2BDA (Watanabe et al., 2018; Dall'Olmo and Gitelson, 2005), and 3BDA algorithms (Abdelmalik, 2018; Gitelson et al., 2003) over the MSI, OLI and OLCI (Ocean and Land Color Instrument) data (Caballero et al., 2020; Pereira Sandoval et al., 2019; Beck et al., 2016). In this study, the mapping of Chl-a of the Al Arish–Al Ghariyah region was carried out by evaluating the performances of 2BDA, 3BDA, NDCI, and FLH violet algorithms based on the field knowledge and visual interpretation of high spatial resolution WorldView-3 data. Initially, we developed single-band output for each algorithm using the Band-Math function and 54 points were sampled from nine selected sites that were comparable to the surface studied in the field and visual interpretation of false-color-composite (FCC, R:7, G:2, B:1) of WorldView-3. Further, the sampling points of MSI data were reviewed for the spectral absorption of Chl-a (as studied above in Fig. 2) and confirmed for the presence of Chl-a in the sampling points. Subsequently, the point data of 3BDA, NDCI, and FLH violet algorithm images of MSI and OLI were collected and analyzed with the point data of WorldView-3 by Pearson linear regression analysis (Beck et al., 2016; Kudela et al., 2015). Table 1 shows the Pearson's test values of different algorithms obtained for MSI and OLI data. The R^2 values indicate

the correlation between the two variables and the change in values between the independent and dependent variables. The values ranging from 0 to 1 are can be described in percentages from 0 to 100%. The study of the results of R^2 values of different algorithms for MSI images shows ranges from 42 to 60% and the NDCI algorithm provided a maximum value when compared with the other algorithms (Table 1). There is no significant difference in the R^2 values between the NDCI and 2BDA algorithms. The 3BDA and FLH violet algorithms show little variation. The R^2 values of all algorithms of the OLI image show poor values and the FLH violet algorithm provides a maximum of 48%, which can be compared and studied with the algorithm of the MSI image. The interpretation of the results shows that all four algorithms of MSI images are better performed when compared with the results of all algorithms for OLI images.

4.2.2. Mapping of Chl-a

We studied the single-band image output of all algorithms for MSI and OLI images of all selected sites. For example, the results of the spatial distribution of Chl-a at the site near Al-Ruwais are given in Fig. 3 (Dashed rectangle in Fig. 1). In the field, the site has a water depth of less than 2 m and contains patches of a mixture of algae, seagrass, plants, and corals. The site is deposited by sediments and is inhabited by a few dead corals. The False-Color Composite (FCC) of WorldView-3 (R:7, G:2, B:1) shows the Chl-a of the site (Fig. 3a) and can be interpreted with the results of the algorithm images of MSI and OLI (Fig. 3b and c). The results of MSI images of the four algorithms (Fig. 3b) show significant correlation and acceptable performance and can be interpreted with the FCC image (Fig. 3a). There is no significant difference between the NDCI and 2BDA images as interpreted above using the R^2 values (Table 1). The image of FLH-violet showed better performance than the image of the 3BDA algorithm in showing the concentration of Chl-a and can be visually interpreted and compared with the FCC image of WorldView-3. The interpretation of all images of OLI by all algorithms (Fig. 3c) shows poor performance except for the result of the FLH violet algorithm, which reflects the maximum value of R^2 (Table 1). The results can be interpreted with the FCC image (Fig. 3a) to understand the performance of the algorithms and OLI data. The study of the images of MSI and OLI of the FLH violet algorithm shows similar performance, which may be due to the utilization of spectral bands in the algorithm. The FLH algorithm measures the green peaks height relative to the red and violet minima within the bands. Overall, the study on the performance of algorithms shows that the NDCI algorithm provided satisfactory performance ($R^2 = 0.6$) over the MSI data to map the concentration of Chl-a. The interpretation of images of MSI and OLI confirms that the MSI image of NDCI shows the best concentration of Chl-a in the site when compared with the other images. The performance of the algorithms may be due to the sensor capability of MSI, which has a relatively high spatial resolution and spectral bandwidth when compared to the resolutions of OLI (see Table 1 in Supplementary material). This study allows us to understand the potential of the four algorithms and the capability of MSI and OLI data to map Chl-a concentrations in Gulf water in the arid region.

4.2.3. Chl-a of Al Arish and Al Ghariyah region

Fig. 4a shows the true-color image (R:4; G:3; B:2) of the study region, which has a very shallow depth to shallow depth of water in light blue to light brownish blue, and the distribution of algae, plants, seagrass, and corals in the water in light green to green. The occurrence of seagrass and corals appears as patchy and spot, respectively, below the water (zoom the image for interpretation). The dissected mud flats developed in the intertidal area over the hard ground carbonate platform by invaded coastal waves can be interpreted from the white tone and warp pattern. The coral reef appears in light brownish green and has developed ridges that protect the inner sea from the distribution of coastal sediments. The gulf water above 2 m appears dark green, which may be due to the penetration of spectral information at a depth of more than 2 m and or the total absorption of light energy in the water (Xu et al., 2019). The coastal region was mapped for Chl-a concentrations using the NDCI, 2BDA, 3BDA, NDCI, and FLH violet algorithms, and the OLI and MSI data. The interpretation of all the images showed that the results of the NDCI-derived MSI image were good for mapping the concentration of Chl-a among the other images. The results obtained using the NDCI algorithm over MSI data are given in Fig. 4b. The image shows the presence of a low concentration of Chl-a < 0.35 μg/L (Fig. 4b). The variation in the concentrations of Chl-a was observed along the coast in the water having a maximum depth of 5 m (Figs. 1 and 4b). However, a significant variation is observed in the concentrations of Chl-a between the coastline of Al Arish to Al Ruwais (west coast region) and Al Ruwais to Al Ghariyah (east coast region) in water having less than 2 m depth.

Over the Al Arish–Al Ruwais coastal water, very poor concentrations of Chl-a were observed in the intertidal area and the area exhibits light green (Fig. 4b). The poor concentration may be due to the presence of sand and mud deposits that occurred at the shallow depth over the carbonate platform, the occurrence of bleached corals, and the erosion and depositional activity of waves and tides that were present over the intertidal area. No concentration was observed on the mudflats. Whereas the coastal region between Al Ruwais and Al Ghariyah shows the presence of a relatively high Chl-a concentration in the region (Fig. 4b), which may be due to the presence of more seagrasses, plants, algae, etc. that occur in the sands on the relatively steep slope which supports the development of phytoplankton (*see* below section). The concentration of Chl-a can be interpreted from the green tone and fine texture. The distribution of Chl-a can be interpreted with the true color image (Fig. 4a). Further, the study of the MSI and OLI images by the FLH violet algorithm (Fig. 4 in Supplementary material) showed a strong correlative relationship in the mapping of Chl-a concentration (as studied above) despite their varying spatial resolutions of 20 m and 30 m, respectively. No significant variation was observed between the two images.

A comparative study of the results derived using MSI sensor with the results of in-situ measurements of Chl-a in the field (*see* the below section) shows that the Chl-a concentration in the coastal water between Al Arish and Al Ghariyah in the Arabian Gulf is very poor, which can be studied with the Bay of North America (Tzortziou et al., 2007), the Baltic Sea (Darecki and Stramski, 2004), the Mediterranean Sea (Di Cicco et al., 2017), and the Chinese coastal waters (Su et al., 2021). The poor concentration of Chl-a in the coastal region is due to the wave and tidal action over the mud that occurred over the wide platform that has a very gentle slope, accumulation of mud, and human interaction apart from the existing climatological factors in the arid environment (Mazière et al., 2022). This study shows the ability of the NDCI algorithm and the capability of MSI data, which has the red-edge, red, and NIR bands to map the Chl-a concentrations.

4.3. Field and laboratory studies

In the field, the beaches and shore areas between Al Arish and Al-Ruwais (west coast region) are wide and very shallow with coastal water and exposed to tidal flooding. The occurrence of mangroves (*Avicennia marina*) (Fig. 5a), the manmade stone barriers for fish and crab catching (Fig. 5b), and the sand containing dead shells of invertebrates (Fig. 5c) were studied in the intertidal

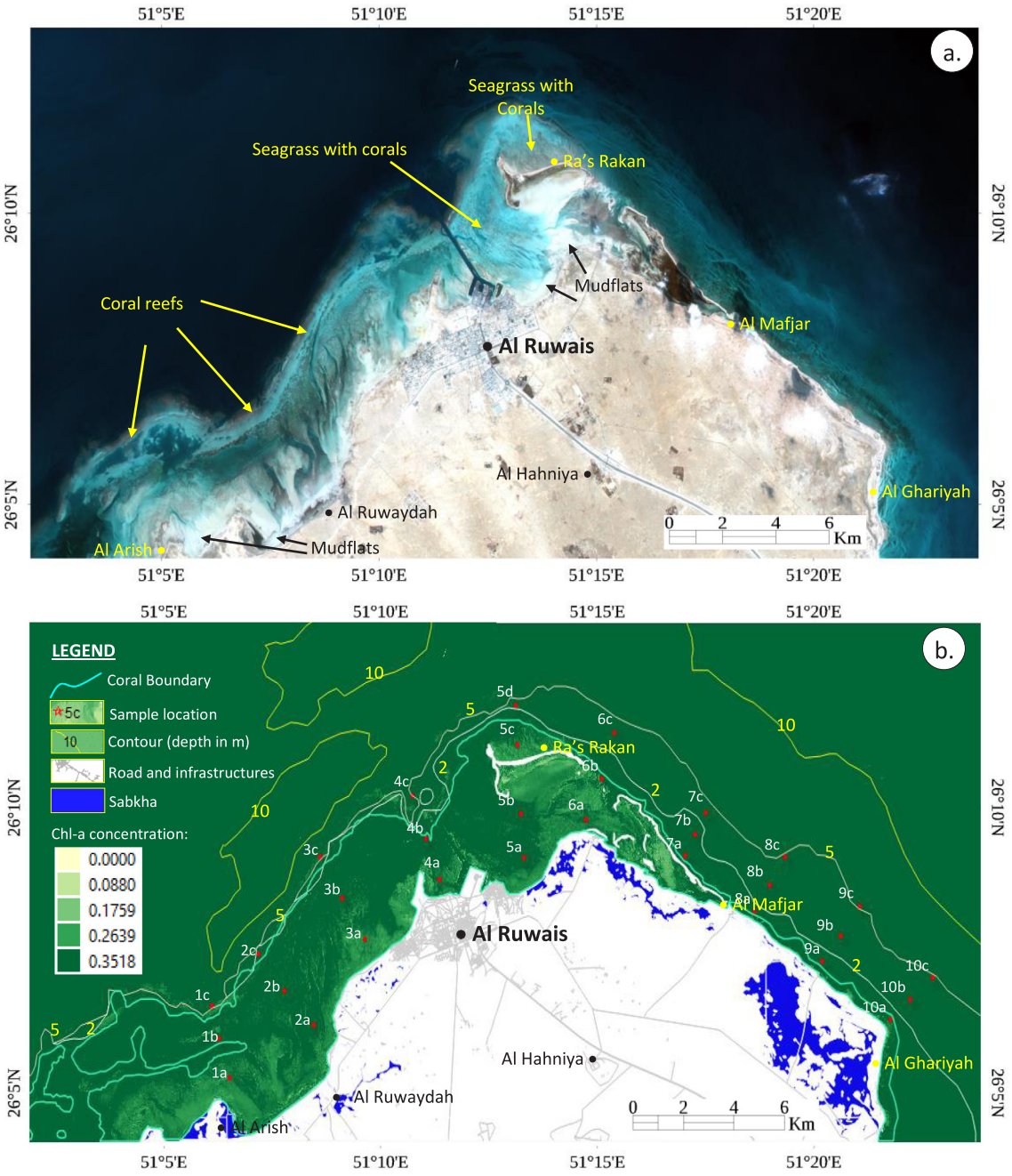

Fig. 4. (a) MSI true-color image (R:4; G:3; B2) showing the occurrence and distribution of seagrass, corals, and plants intervened by sediments in the shallow coastal water in the shades of light greenish-blue along the Al Arish–Al Ghariyah coastal region, and (b) NDCI image of MSI showing the Chl-a concentration along the region. . (For interpretation of the references to color in this figure legend, the reader is referred to the web version of this article.)

zone, shore, and beach areas. We observed the presence of a very low distribution of algal cells and filaments in the coastal water column and that the poor distribution is due to wave and tide activity in the very shallow water over the mudflats (Fig. 5a, b, and c). The presence of fewer live and more sponges (*Axinyssa aplysinoides* and *Callyspongia* sp.) (Fig. 5d), and bleached plants (*Dictyosphaeria cavernosa* and hydrozoa *Dynamena pumila*) (Fig. 5e) and seagrass are studied underwater. Among these, most of them are degraded (Fig. 5f) due to bleaching and anthropogenic activities that include fishing and coastal development (Burt et al., 2016; Purkis and Riegl, 2012; Sheppard et al., 2010). We also observed the presence of dead shells such as *Galeolaria caespitosa, Euchelus asper, Pinctada radiata, Neotrapezium sublaevigatum,* and *Pinna bicolor* on the beach (Fig. 7a, b, and c in Supplementary material), the dead algae, chordata and sea sponge including the *Digenea simplex*, *Eudistoma* sp., *Haliclona* sp. (Fig. 7d, e and f in Supplementary material) over the clay bed in the intertidal zone and beach areas. Very poor occurrence of macroalgae over the carbonate formations, boulders, and sediments are observed underwater along the channel developed due to backwater erosional activity during low tide rather than the bleached plants (Fig. 7 g, h in Supplementary material) and dead seagrass deposits along the beach (Fig. 7i in Supplementary material). Research studies have demonstrated that the coral reefs in the Gulf have widely degraded in the past three decades and the extensive losses resulted due to large-scale bleaching events that occurred during warm summers (Riegl and Purkis, 2012; Sheppard et al., 2010).

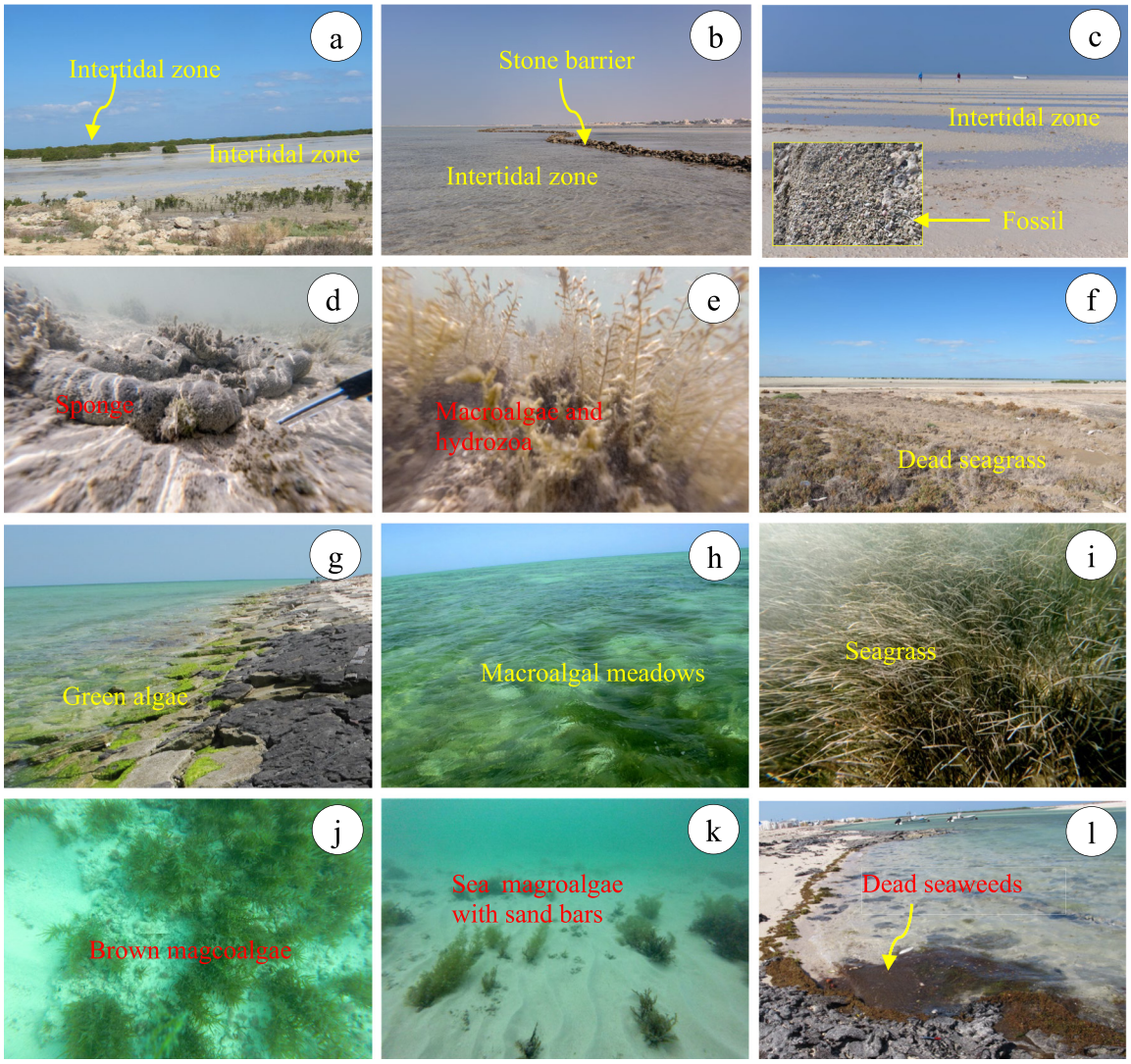

Fig. 5. Field photographs show the occurrence of (a) mangroves, (b) manmade stone barriers, and (c) clay deposits in the intertidal zone, the presence of (d) dead corals, (e) bleached plants underwater and the occurrence of (f) dead seagrass and plant deposits along the beach in the Al Arish–Al Ruwais coastal region; and the field photograph showing the occurrence of (g) green algae over carbonate rocks, the presence of (h) macroalgal meadows (Turf Seaweeds), (i) and (j) seagrass and plants, (k) plants with sand bars underwater and (l) the algae and plants along the beach in the Al Ruwais–Al Ghariyah coastal region.

Whereas, in the coastal region between Al-Ruwais and Al Ghariyah (east coast region), the growth of algae (*Chlorophyta*), and the occurrence of a high density of macroalgae over the massive beds of limestone are studied (Fig. 5g). The presence of macroalgal meadows and Turf Seaweeds are frequently observed underwater all along the coast where the water depth is less than 1 m (Fig. 5h). More occurrences of seagrass and plants (*Halodule uninervis*, *Hormophysa cuneiformis*, *Sirophysalis trinodis*) underwater over the sediments studied along the coast have less than 2 m water depth (Fig. 5i and k). The seagrass beds have heterogeneous distributions of macroalgal beds and are often intermixed with sand. The seagrass beds stabilize sediment by their root system and protect against erosion in this region. Sheppard et al. (2010) stated the presence of four seagrass species, namely the *Halodule uninervis, Syringodium isoetifolium, Halophila ovalis*, and *Halophila stipulacea* in the gulf region (Erftemeijer and Shuail, 2012). They are a direct food source for many herbivores and provide indirect energy to the detrital food web and nursery habitats for a variety of commercially important fishes. The occurrence of sand bars developed due to current activity and the presence of sea macroalgae over sand was studied underwater having a depth of more than 2 m (Fig. 5j). The presence of algae that were not caused by bleaching (Fig. 5l) was observed along the intertidal zone. The offshore areas are rich in algae, plants, and grasses (Fig. 7j in Supplementary material) and the presence of live fossils (*Planaxis sulcatus*), fishes, crabs (*Portunus segnis)*, turtles, sea urchins (*Echinometra mathaei*) (Fig. 7k, l, and m in Supplementary material) and wales are studied. The growth of grass over the sands (Fig. 7n in Supplementary material) in the intertidal zone and the growth of different plants (Fig. 7o in Supplementary material) underwater were studied in the Al Ruwais–Al Ghariyah coastal region. All these occurrences indicate that the coast is relatively rich in Chl-a and nutrients when compared to the Al Arish–Al Ruwais coastal region.

Further, the in-situ measurements of temperature (T), electrical conductivity (Ec), hydrogen ion concentration (pH), total dissolved solids (TDS), and Chlorophyll-a (Chl-a) were carried out in the coastal surface water at the study sites between Al Arish and Al Ghariyah (Table 2) and studied for their spatial distributions and concentrations. The measurements of temperature, EC, pH, and TDS provided the minimum and maximum range values as 19 to 29.9 °C, 45 896 to 70 941 μS/cm, 7.86 to 8.17, and 25795 to 38 795 g/L respectively (Table 2). The study of the spatial distribution of temperature, Ec, pH, and TDS shows that these

Table 3
Selected major and trace elements concentrations in the surface coastal water of the Al Arish-Al Ghariyah region of northern Qatar.

Sample No	Depth (m)	K	Ca	Na	Mg	Al	Fe	Mn	Cl	HCO3	SO4	Cu	Pb	Cr	Ni	Sr	Zn
		Major cation							Major anion			Trace elements					
		(in mg/l)										(in ppb)					
la		431.22	351.05	10 158.91	1031.06	n.d.	0.0504	0.0067	35 218.58	190.47	2164.72	22.9	3	n.d	n.d	6826.9	72.7
lb		447.21	330.42	7737.06	1129.85	n.d.	0.0138	0.0057	34 812.71	168.25	2099.15	8.4	n.d	n.d	n.d	7207	12.7
lc		634.37	506.36	13 444.07	1350.38	n.d.	0.0512	0.0092	34 307.91	157.14	2099.15	5.3	n.d	n.d	0.8	9381.2	24
2a		509.93	341.95	7736.12	1121.66	0.0392	0.2272	0.0085	37 039.91	201.58	2082.75	27	6.7	n.d	n.d	6885.3	66.7
2b		464.62	331.16	8144.09	915.63	0.0718	0.0439	0.0088	35 841.17	151.58	2181.11	11.9	23.6	n.d	11.3	5733.2	28.7
2c		556.59	427.36	12 829.84	1137.85	0.0557	0.0301	0.0081	34 159.23	134.92	2131,93	11	12.8	n.d	11.7	7864.7	44.6
3a		489.09	329.52	10 654.15	925.43	0.0802	0.0305	0.0079	35 850.47	190.47	2148.33	9.6	40.9	n.d	n.d	6155.1	37.9
3b		504.35	343.88	9166.12	961.59	n.d.	0.0979	0.0078	35 116.36	159.92	2246.69	4.3	n.d	n.d	n.d	6033.8	43.4
3c		710.26	535.94	8685.17	1338.28	n.d.	0.0151	0.0093	34 149.94	137.69	2131.93	29.4	n.d	n.d	n.d	9031.6	68.3
4a		430.62	300.46	9894.69	729.48	0.0395	0.0092	0.0176	34 205.69	104.36	2246.69	57.2	44	n.d	n.d	4754.4	63
4b		414.92	297.86	10 073.67	786.28	n.d.	0.0316	0.0084	34 233.57	107.14	2328.66	1.5	2.6	n.d	n.d	5104.6	18
4c		459.23	337.73	10 170.2	992.12	n.d.	n.d.	0.008	34 410.13	137.69	2328.66	3.8	10.2	n.d	n.d	6404.7	67.1
5a		301.65	328.45	7099.63	564.47	n.d.	0.0551	0.0109	34 857.23	143.25	2279.48	25.8	2.1	n.d	6.3	5887.7	41.8
5b		138.65	118.63	2750.01	280.41	0.1018	0.0089	0.0062	33 099.89	159.92	2181.11	29	16.3	2.5	n.d	1920.9	71.7
5c		497.62	348.22	9838.18	965.64	n.d.	0.0104	0.0107	34 391.54	159.92	2131.93	34.2	n.d	n.d	5.4	6375.6	45.2
5d	Less than 0.5 m	539.94	405.52	9485.03	986.58	n.d.	n.d.	0.0118	34 465.88	151.58	2181.11	19.6	3.3	n.d	n.d	6633.8	24.9
6a		424.22	308.70	8285.77	726.22	n.d.	0.0012	0.0133	35 004.85	193.25	2246.69	28.4	11.4	n.d	n.d	4550.7	95.9
6b		335.50	238.32	7711.78	526.64	0.0243	n.d.	0.0087	34 177.82	193.25	2263.08	18.7	50.2	n.d	n.d	3424.5	12.2
6c		492.72	338.19	8881.33	866.97	n.d.	n.d.	0.01	34 190.5	193.25	2230.3	14.1	n.d	n.d	n.d	5387.1	7.7
7a		368.02	278.17	7439.17	795.87	n.d.	n.d.	0.0071	34 428.71	146.03	2197.51	0.1	n.d	n.d	7.1	5225.7	3.3
7b		345.56	258.38	7886.61	632.78	n.d.	0.0223	0.009	34 196.4	154.36	2230.3	18.3	3.3	n.d	2	4060.8	80.9
7c		477.47	340.17	11 591.66	808.28	n.d.	n.d.	0.0098	34 001.26	134.92	2181.11	13.9	n.d	n.d	n.d	5173.2	7.1
8a		134.77	111.08	2381.84	256.66	0.1237	n.d.	0.0059	32 802.53	162.69	2246,69	18.1	25.1	0.04	4.3	1668.5	20.1
8b		471.74	334.89	10 529.2	877.50	0.0911	n.d.	0.0105	33 322.91	162.69	2197.51	19	n.d	n.d	n.d	5443.7	67.8
8c		564.80	419.87	10 115.55	1066.55	0.0232	n.d.	0.0066	33 276.44	151.58	2246.69	n.d	3.4	n.d	n.d	6957	44.9
9a		299.40	205.81	6096.80	500.30	n.d.	n.d.	0.0038	32 486.58	123.81	219 731	n.d	1.9	n.d	7.3	3156.1	29.9
9b		200.82	147.07	4146.35	402.89	0.2062	n.d.	0.0038	32 858.28	148.81	2213.9	8.7	6.1	n.d	n.d	2315.9	58.1
9c		455.82	336.18	9773.41	821.41	n.d.	n.d.	0.0055	32 709.6	151.58	2246.69	n.d	n.d	n.d	n.d	5522.3	n.d
10a		257.68	200.58	3074.06	420.62	0.0796	n.d.	0.0031	32 272.85	140.47	2246.69	n.d	4.1	2.7	5.8	2460.8	40
10b		441.96	324.21	7371.25	751.96	0.0465	0.0053	0.0054	32 274.33	140.47	2279.48	10.9	6.9	n.d	n.d	4811.4	44.8
10c		446.58	323.89	9612.72	811.88	0.0351	0.0195	0.0061	32 941.91	104.36	2279.48	n.d	n.d	n.d	n.d	5324.1	21

are relatively high in the coastal region between Al Arish and Al Ruwais when compared with the region between Al Ruwais and Al Ghariyah (Fig. 5a to d in the Supplementary material) as studied by Ibrahim et al. (2020), Kampf and Sadrinasab (2006), and Sultan and Elghribi (1996). The measurement of Chl-a showed the presence of low concentration in the range from 0.0491 to 0.5512 μg/L (Table 2) as interpreted over the satellite image (Fig. 4b). The map prepared for the spatial distribution of Chl-a in the region showed the presence of such a low concentration between the Al Arish and Al Ghariyah coastal waters (Fig. 5e in the Supplementary material). The concentration is relatively low along the coastal region between Al Arish and Al Ruwais when compared with the region between Al Ruwais and Al Ghariyah. The map depicts the occurrence of a relatively high concentration of Chl-a in the water where the presence of a high biomass of phytoplankton is in the water.

Moreover, the analysis of water samples in the laboratory for the concentration of major and trace elements in the coastal region showed the enrichment of elements in the decreasing order of Ca>Mg>K>Na. The maximum and minimum values were 535 and 111, 1338 and 256, 634 and 138, and 13444 and 2381 mg/l respectively (Table 3; Fig. 6 in Supplementary material) (El Din et al., 2005; Habib et al., 2002). The presence of poor concentrations of Al, Fe, and Mn was observed in the water. The concentrations of elements may be due to the occurrence and interaction of water over the mud-deposited carbonate platform (El Din et al., 2005; Gouda et al., 1993). The interpretation of data is comparable with the study on the formation and circulation of dense water in the Persian/Arabian Gulf that was carried out by El Din et al. (2005), Habib et al. (2002), and Swift and Bower (2003). In addition, the samples showed the presence of poor concentrations of trace elements in the decreasing order of Sr>Zn> Cu> Pb>Ni>Cr (Table 3). Most of the samples showed the presence of Sr, Zn, Mn, and Cu elements. The elements such as Al, Fe, and Pb are present at relatively high concentrations, but most samples show absence in their concentrations. Such concentrations were observed in the samples that were collected over the intertidal zone where the mud deposits have occurred. The concentrations of Ni and Cr are absent in almost all samples, which represent the occurrence of water over the sedimentary carbonate formations.

5. Discussion

Agha et al. (2012) stated that Chl-a concentrations move vertically along the water column and vary in time and space, and thus the detecting of Chl-a through in-situ measurements is challenging, especially where the limited infrastructure to measure data. Literature reviews that several factors, including the upwelling and downwelling phenomena, determine the primary biological production in the eastern Arabian Sea (Shah et al., 2019; Luis and Kawamura, 2004). Studies have also discussed the increase in chlorophyll concentration due to the input of nutrients from terrestrial sources to coastal water (Shah et al., 2019; Shafeeque et al., 2019). In this study, the MSI and OLI data, and the algorithms such as NDCI, 2BDA, 3BDA, and FLH-violet were used to map the concentrations of Chl-a in the coastal region of Al Arish–Al Ghariyah in the northern part of Qatar by evaluating the algorithms using field knowledge and high spatial resolution satellite data. The study showed the best performance of NDCI (R^2 = 60%) over the MSI data when compared to other algorithms. The interpretation of the MSI showed the presence of a very poor concentration of Chl-a in the Al Arish–Al Ruwais, where the area has a very gentle slope, water having a 2 m depth, and active erosion and deposition when compared with the Al Ruwais–Al Ghariyah which has a relatively high concentration of Chl-a due to the occurrences of more algae, plants, and seagrasses. No concentration of Chl-a over the mudflats was observed in the coastal region between Al Arish and Al Ruwais. However,

the mapping of Chl-a of the region depends on the resolution of sensors; the use of data that is acquired on closer dates instead of the same day for in-situ measurements, and the performance of the preprocessing of data, which includes atmospheric correction. It should be noted that the positions, bandwidths, and SNR of the MSI and OLI have differences, and that the NDCI algorithm uses red and red-edge spectral bands when compared to the other algorithms.

The results for mapping of Chl-a in the study area were validated through field studies, in-situ measurements, and water sample analyses. The field studies support that the Al Arish and Al Ruwais coastal region occurred with a poor concentration of Chl-a when compared with the coastal region between Al-Ruwais and Al Ghariyah, since the region occurs with the high density macroalgal, seagrass, and plants and presence of live fossils. The results have been studied with in-situ measurements of temperature, Ec, pH, TDS, and Chl-a. Importantly, the map prepared for the spatial distribution of Chl-a confirmed the presence of a low concentration of Chl-a in the west coastal region and a relatively high concentration of Chl-a in the east coastal region. Moreover, the analysis of surface water samples for major elements concentration showed the decreasing order of Ca>Mg>K>Na elements concentration with the presence of a poor concentration of trace elements that was comparable with earlier studies. Overall, this study shows that the MSI data and the NDCI algorithm are more suitable for the mapping of Chl-a concentrations in the water of the Arabian Gulf when compared to the OLI data and other algorithms used in this study.

6. Conclusions

In this study, we described the spectral band absorptions of Chl-a, which has unique spectral absorptions near 440, 475, and 670 nm in the blue and red regions and a peak reflectance around 500 and 700 nm in the green and NIR regions. Based on this, we detected the presence of Chl-a in the Al Ghariyah using hyperspectral Hyperion data via the LUS method and mapped the concentrations of Chl-a in the Al Arish–Al Ghariyah coastal region of Qatar in the Arabian Gulf using MSI and OLI data by NDCI, 2BDA, 3BDA, and FLH violet algorithms. We evaluated the performance of the algorithms using high spatial resolution WorldView-3 data and field knowledge, which showed that the NDCI algorithm performed best ($R^2 = 60\%$) over the MSI data when compared to the other algorithms. The MSI image obtained based on the NDCI algorithm showed the presence of poor concentrations of Chl-a in the coastal region. A comparative study on the concentrations of Chl-a between Al Arish–Al Ruwais and Al Ruwais–Al Ghariyah showed that the Al Ruwais–Al Ghariyah region has a relatively high concentration of Chl-a in the region. The results of the satellite data were validated through field studies, in-situ measurements of temperature, Ec, pH, TDS, and Chl-a, and laboratory analyses of water samples for the concentrations of major and trace elements. This study assessed the concentrations of Chl-a in the study region and recommends the algorithm and the data that could be used as a tool for mapping and monitoring the Chl-a of the gulf water of similar regions in the world.

CRediT authorship contribution statement

Sankaran Rajendran: Conceptualization, Methodology, Data curation, Writing - original draft. **Noora Al-Naimi:** Data curation, Writing – review & editing. **Jassim A. Al Khayat:** Investigation, Visualization, Writing – review & editing. **Caesar Flonasca Sorino:** Data curation, Formal analysis. **Fadhil N. Sadooni:** Visualization, Writing – review & editing. **Hamad Al Saad Al Kuwari:** Visualization, Writing – review & editing.

Declaration of competing interest

The authors declare that they have no known competing financial interests or personal relationships that could have appeared to influence the work reported in this paper.

Data availability

Data will be made available on request.

Acknowledgments

Open Access funding provided by the Qatar National Library. This study is supported by Qatar University Grant no. QUEX-ESC-QAFCO-20/21-1. The authors are thankful for the USGS Data Management and Information Distribution (DMID) (https://glovis.usgs.gov/) for sharing the Hyperion and Landsat-8 data, and the Copernicus, European Space Agency for sharing the Sentinel-2 data through sentinel open access hub (https://sentinel.esa.int/web/sentinel/sentinel-data-access). The Digital Globe, USA is acknowledged for providing the WorldView-2 satellite image (Image ID: 104001004D7C7D00) that was acquired on n June 29, 2019. Mr. Fahad Syed Asim, Mr. Faisal Muthar Al-Quaiti, and Mr. Reyniel M. Gasang are thanked for their support in the fieldwork. Mr. Mark Edward Chatting is thanked for taking underwater photography and collecting underwater samples. The sediments, water, and biological samples for different analyses are organized by Ms. Thoraya Haidar S A Alyafei. The classification and naming of biological samples are provided by Ms. Aisha Ahmed Al Ashwal. Mr. Hamood Abdulla Alsaadi and Ms. Marwa Mustufa Al-Azhari have analyzed water samples for major and trace element concentrations. The authors are thankful to Prof. Seongjin Hong, the Associate Editor and anonymous reviewer of the journal for the valuable reviews, providing comments and suggestions that have helped to present the work lucidly.

Appendix A. Supplementary data

Supplementary material related to this article can be found online at https://doi.org/10.1016/j.rsma.2022.102680.

References

Abbas, M.M., Melesse, A.M., Scinto, L.J., Rehage, J.S., 2019. Satellite estimation of chlorophyll-a using moderate resolution imaging spectroradiometer (MODIS) sensor in Shallow Coastal water bodies: Validation and improvement. Water 11, 1621.

Abdelmalik, K., 2018. Role of statistical remote sensing for Inland water quality parameters prediction. Egypt. J. Remote Sens. Space Sci. 21, 193–200.

Abuzied, S.M., Ibrahim, S.K., Kaiser, M.F., Seleem, T.A., 2016. Application of remote sensing and spatial data integrations for mapping porphyry copper zones in Nuweiba area. Egypt. Int. J. Signal Process. Syst. 4 (2), 102–108.

Agha, R., Cires, S., Wörmer, L., Domínguez, J.A., Quesada, A., 2012. Multi-scale strategies for the monitoring of fresh-water cyanobacteria: Reducing the sources of uncertainty. Water Res. 46, 3043–3053.

Al-Naimi, N., Raitsos, D.E., Ben-Hamadou, R., Soliman, Y., 2017. Evaluation of satellite retrievals of chlorophyll-a in the Arabian Gulf. Remote Sens. 9, 301.

Al Senafi, F., Anis, A., 2015. Shamals and climate variability in the Northern Arabian/Persian Gulf from 1973 to 2012. Int. J. Climatol. 35, 4509–4528.

Alawadi, F., 2010. Detection of surface algal blooms using the newly developed algorithm surface algal bloom index (SABI). Remote Sens. Ocean Sea Ice Large Water Reg. 7825, 7782506.

Anderson, G.P., Felde, G.W., Hoke, M.L., Ratkowski, A.J., Cooley, T.W., James, H., Chetwynd, J., Gardner, J.A., Adler-Golden, S.M., Matthew, M.W., Berk, A., Bernstein, L., Acharya, P.K., 2002. MODTRAN4-based atmospheric correction algorithm: FLAASH (fast line-of-sight atmospheric analysis of spectral hypercubes). Proc. SPIE-Int. Soc. Opt. Eng. 4725, 65–71.

Ansper, A., Alikas, K., 2019. Retrieval of chlorophyll-a from sentinel-2 MSI data for the European union water framework directive reporting purposes. Remote Sens. 11, 64.

Beck, R.A., Zhan, S., Liu, H., Tong, S.T.Y., Yang, B., Xu, M., Ye, Z., Huang, Y., Shu, S., Wu, Q., et al., 2016. Comparison of satellite reflectance algorithms for estimating chlorophyll-a in a temperate reservoir using coincident hyperspectral aircraft imagery and dense coincident surface observations. Remote Sens. Environ. 178, 15–30.

Boucher, J., Weathers, K.C., Norouzi, H., Steele, B., 2018. Assessing the effectiveness of landsat 8 chlorophyll-a retrieval algorithms for regional freshwater monitoring. Ecol. Appl. 28, 1044–1054.

Buma, W.G., Lee, S.-I., 2020. Evaluation of sentinel-2 and landsat 8 images for estimating chlorophyll-a concentrations in Lake Chad, Africa. Remote Sens. 12, 2437.

Burt, J.A., 2014. The environmental costs of coastal urbanization in the Arabian Gulf. City 18, 760–770.

Burt, J.A., Smith, E.G., Warren, C., Dupont, J., 2016. An assessment of Qatar's coral communities in a regional context. Mar. Pollut. Bull. 105, 473–479.

Caballero, I., Fernández, R., Escalante, O.M., Maman, L., Navarro, G., 2020. New capabilities of sentinel-2A/B satellites combined with in situ data for monitoring small harmful algal blooms in complex coastal waters. Sci. Rep. 10, 8743.

Cavalcante, G.H., Feary, D.A., Burt, J.A., 2016. The influence of extreme winds on coastal oceanography and its implications for coral population connectivity in the southern Arabian Gulf. Mar. Pollut. Bull. 105, 489–497.

Chen, J., Zhu, W., Tian, Y.Q., Yu, Q., Zheng, Y., Huang, L.l., 2017. Remote estimation of colored dissolved organic matter and chlorophyll-a in Lake Huron using Sentinel-2 measurements. J. Appl. Remote Sens. 11, 036007.

Cherif, E.K., Mozetič, P., Francé, J., Flander-Putrle, V., Faganeli-Pucer, J., Vodopivec, M., 2021. Comparison of in situ chlorophyll-a time series and sentinel-3 ocean and land color instrument data in Slovenian National Waters (Gulf of Trieste, Adriatic Sea). Water 13, 1903.

Clevers, J.G.P.W., Gitelson, A.A., 2013. Remote estimation of crop and grass chlorophyll and nitrogen 682 content using red-edge bands on Sentinel-2 and -3. Int. J. Appl. Earth 683 Obs. Geoinf. 23, 344–351.

Cordero-Bailey, K., Bollozos, I.F., Palermo, J.h., Silvano, K.M., Escobar, M.L., Jacinto, G.s., Diego-McGlone, M.S., David, L.T., Yñiguez, A.T., 2021. Characterizing the vertical phytoplankton distribution in the Philippine Sea off the northeastern coast of Luzon. Estuar. Coast. Shelf Sci. 254, 107322.

Dall'Olmo, G., Gitelson, A.A., 2005. Effect of bio-optical parameter variability on the remote estimation of chlorophyll-a concentration in turbid productive waters: Experimental results. Appl. Opt. 44, 412–422.

Darecki, M., Stramski, D., 2004. An evaluation of MODIS and SeaWiFS bio-optical algorithms in the Baltic Sea. Remote Sens. Environ. 89, 326–350.

Di Cicco, A., Sammartino, M., Marullo, S., Santoleri, R., 2017. Regional empirical algorithms for an improved identification of Phytoplankton functional types and size classes in the Mediterranean Sea using satellite data. Front. Mar. Sci. 4.

Doerffer, R., 1981. Factor analysis in ocean color interpretation. In: Gower, J.F.R. (Ed.), Oceanography from Space. Plenum Press, New York, pp. 339–345.

Drusch, M., Del Bello, U., Carlier, S., Colin, O., Fernandez, V., Gascon, F., et al., 2012. Sentinel-2: Esa's optical high-resolution mission for GMES operational services. Remote Sens. Environ. 120, 25–36.

El Din, A.M.S., El-Dahshan, M.E., Mohammed, R.A., 2005. Scale formation in flash chambers of high-temperature MSF distillers. Desalination 177 (1–3), 241–258.

Erftemeijer, P.L.A., Shuail, D.A., 2012. Seagrass habitats in the Arabian Gulf: distribution, tolerance thresholds and threats. Aquat. Ecosyst. Health Manage. 15 (1), 73–83.

ESA, 2015. European Space Agency. Sentinel-2 User HandBook. ESA Standard Document, European Space Agency, Paris, France.

Fu, Y., s, Xu., Zhang, C., Sun, Y., 2018. Spatial downscaling of MODIS Chlorophyll-a using landsat 8 images for complex coastal water monitoring. Estuar. Coast. Shelf Sci. 209, 149–159.

Gao, Z-Y., Wang, S-C., Zhang, Y-X., Liu, F-F., 2022. Single and combined toxicity of polystyrene nanoplastics and copper on Platymonas helgolandica var, tsingtaoensis: Perspectives from growth inhibition, chlorophyll content and oxidative stress. Sci. Total Environ. 829, 154571.

George, G., 2014. Numerical modelling and satellite remote sensing as tools for research and management of marine Fishery resources. In: Finkl, C., Makowski, C. (Eds.), Remote Sensing and Modeling. In: Coastal Research Library, vol. 9, Springer, Cham, pp. 431–452. http://dx.doi.org/10.1007/978-3-319-06326-3_18.

Gernez, P., Doxaran, D., Barillé, L., 2017. Shellfish aquaculture from space: Potential of Sentinel2 to monitor tide-driven changes in turbidity, chlorophyll concentration and oyster physiological response at the scale of an oyster farm. Front. Mar. Sci. 4.

Gitelson, A., 1992. The peak near 700 nm on radiance spectra of algae and water: relationships of its magnitude and position with chlorophyll concentration. Int. J. Remote Sens. 13, 3367–3373.

Gitelson, A.A., Gritz, U., Merzlyak, M.N., 2003. Relationships between leaf chlorophyll content and spectral reflectance and algorithms for non-destructive chlorophyll assessment in higher plant leaves. J. Plant Physiol. 160, 271–282.

Gons, H.J., Rijkeboer, M., Ruddick, K.G., 2002. A chlorophyll-retrieval algorithm for satellite imagery (Medium Resolution Imaging Spectrometer) of inland and coastal waters. J. Plankton Res. 24 (9), 947–951.

Goodenough, D.G., Dyk, A., Niemann, K.O., Pearlman, J.S., Chen, H., Han, T., Murdoch, M., West, C., 2003. Processing Hyperion and Ali for forest classification. IEEE Trans. Geosci. Remote Sens. 41, 1321–1331.

Gouda, V.K., Banat, I.M., Riad, W.T., Mansour, S., 1993. Microbiologically induced corrosion of UNS N04400 in seawater. Corrosion 49 (1), 63–73.

Gower, J.F.R., 1980. Observations of in situ fluorescence of chlorophyll-a in Saanich Inlet. Boundary-Layer. Meteorol. 18, 235–245.

Grendaitė, D., Stonevičius, E., Karosiene, J., Savadova, K., Kasperovičienė, J., 2018. Chlorophyll-a concentration retrieval in eutrophic lakes in Lithuania from Sentinel-2 data. Geol. Geogr. T 4 (1), 15–28.

Habib, K., Riad, W., Muhanna, K., Al-Sumait, H., 2002. Electrochemical behavior of Al-brass in polluted natural seawater. Desalination 142, 5–9.

Hao, Q., Chai, F., Xiu, P., Bai, Y., Chen, J., Liu, C., Le, F., Zhou, F., 2019. Spatial and temporal variation in chlorophyll a concentration in the eastern China seas based on a locally modified satellite dataset. Estuar. Coast. Shelf Sci. 220, 220–231.

He, J., Christakos, G., Wu, J., Li, M., Leng, J., 2021. Spatiotemporal BME characterization and mapping of sea surface chlorophyll in Chesapeake Bay (USA) using auxiliary sea surface temperature data. Sci. Total Environ. 794, 148670.

Hu, M., Zhang, Y., Ma, R., Xue, K., Cao, Q., Jing, Y., 2021. Optimized remote sensing estimation of the lake algal biomass by considering the vertically heterogeneous chlorophyll distribution: Study case in Lake Chaohu of China. Sci. Total Environ. 771, 144811.

Hussein, K.A., Al Abdouli, K., Ghebreyesus, D.T., Petchprayoon, P., Al Hosani, N.O., Sharif, H., 2021. Spatiotemporal variability of chlorophyll-a and sea surface temperature, and their relationship with bathymetry over the coasts of UAE. Remote Sens. 13, 2447.

Ibrahim, H.D., Xue, P., Eltahir, E.A.B., 2020. Multiple salinity equilibria and resilience of Persian/Arabian Gulf Basin salinity to Brine Discharge. Front. Mar. Sci. 7, 573.

Ismail, S.S., Ramli, N.H., Semawi, N.M., Abdul Kadir, M.Z., Ali, A.N., 2020. Variations in physico-chemical parameters and Chl-a concentration in Setiu Wetlands lagoon during the northeast and inter-monsoon seasons 2018. IOP Conf. Ser.: Earth Environ. Sci. 494, 012014.

John, V., Coles, S., Abozed, A., 1990. Seasonal cycles of temperature, salinity and water masses of the western Arabian Gulf. Oceanol. Acta 13, 273–281.

Joydas, T.V., Qurban, M.A., Manikandan, K.P., Ashraf, S.M., Al-Abdulkader, K., Qasem, A., Krishnakumar, P.K., 2015. Status of macrobenthic communities in the hypersaline waters of the Gulf of Salwa, Arabian Gulf. J. Sea Res. 99, 34–46.

Kampf, J., Sadrinasab, M., 2006. The circulation of the Persian gulf: A numerical study. Ocean Sci. 2, 27–41.

Katlane, R., Dupouy, C., El Kilani, B., Berges, J.C., 2020. Estimation of chlorophyll and turbidity using sentinel 2A and EO1 data in Kneiss Archipelago Gulf of Gabes, Tunisia. Int. J. Geosci. 11, 708–728.

Kirk, J.T., 1994. Light and Photosynthesis in Aquatic Ecosystems. Cambridge University Press.

Kudela, R.M., Palacios, S.L., Austerberry, D.C., Accorsi, E.K., Guild, L.S., Torres-Perez, J., 2015. Application of hyperspectral remote sensing to cyanobacterial blooms in inland waters. Remote Sens. Environ. 1–10.

Li, X., Sha, J., Wang, Z.-L., 2017. Chlorophyll-A prediction of lakes with different water quality patterns in China based on hybrid neural networks. Water 9, 524.

Lins, R.C., Martinez, J.M., Marques, D.D., Cirilo, J.A., Fragoso, C.R., 2017. Assessment of chlorophyll-a remote sensing algorithms in a productive tropical estuarine-lagoon system. Remote Sens. 9, 516.

Liu, H., Li, Q., Shi, T., Hu, S., Wu, G., Zhou, Q., 2017. Application of Sentinel 2 MSI images to retrieve suspended particulate matter concentrations in Poyang Lake. Remote Sens. 9 (7), 761.

Lokier, S.W., Fiorini, F., 2016. Temporal evolution of a coastal system, Abu Dhabi, United Arab Emirates. Mar. Geol. 381, 102–113.

Lokier, S.W., Knaf, A., Kimiagar, S., 2013. A quantitative analysis of recent arid coastal sedimentary facies from the Arabian Gulf Coastline of Abu Dhabi, United Arab Emirates. Mar. Geol. 346, 141–152.

Louis, J., Debaecker, V., Pflug, B., Main-Knorn, M., Bieniarz, J., Müller-Wilm, U., Cadau, E., Gascon, 773.F., 2016. SENTINEL-2 SEN2COR: L2A processor for users.

Lu, X., Liu, C., Niu, Y., Yu, S., 2021. Long-term and regional variability of phytoplankton biomass and its physical oceanographic parameters in the Yellow Sea, China. Estuar. Coast. Shelf Sci. 260, 107497.

Luis, A.J., Kawamura, H., 2004. Air-sea interaction, coastal circulation and biological production in the Eastern Arabian Sea: A review. J. Oceanogr. 60 (2), 205–218.

Madhupratap, M., Kumar, S.P., Bhattathiri, P.M.a., Kumar, M.D., Raghukumar, S., Nair, K.K.C., Ramaiah, N., 1996. Mechanism of the biological response to winter cooling in the northeastern Arabian Sea. Nature 384 (6609), 549–552.
Matthews, M.W., 2011. A current review of empirical procedures of remote sensing in Inland and near-coastal transitional waters. Int. J. Remote Sens. 32, 6855–6899.
Mazière, C., Bodo, M., Perdrau, M.A., Cravo-Laureau, C., Duran, R., Dupuy, C., Hubas, C., 2022. Climate change influences chlorophylls and bacteriochlorophylls metabolism in hypersaline microbial mat. Sci. Total Environ. 802, 149787.
Méléder, V., Barillé, L., Rincé, Y., Morançais, M., Rosa, P., Gaudin, P., 2005. Spatio-temporal changes in microphytobenthos structure analysed by pigment composition in a macrotidal flat (Bourgneuf Bay, France). Mar. Ecol. Prog. Ser. 297, 83–99.
Mishra, S., Mishra, D.R., 2012. Normalized difference chlorophyll index: A novel model for remote estimation of chlorophyll-a concentration in turbid productive waters. Remote Sens. Environ. 117, 394–406.
Mohamed, E., Ioannis, G., Anas, O., Jarbou, B., Petros, G., 2019. Assessment of water quality parameters using temporal remote sensing spectral reflectance in arid environments, Saudi Arabia. Water 11, 556.
Moses, W.J., Saprygin, V., Gerasyuk, V., Povazhnyy, V., Berdnikov, S., Gitelson, A.A., 2019. OLCI-based NIR-red models for estimating chlorophyll-a concentration in Productive Coastal waters—a preliminary evaluation. Environ. Res. Commun. 1, 011002.
Pahlevan, N., Lee, Z.-P., Wei, J., Schaaf, C.B., Schott, J.R., Berk, A., 2014. On-orbit radiometric characterization of OLI (landsat-8) for applications in aquatic remote sensing. Remote Sens. Environ. 154, 272–284.
Pahlevan, N., Smith, B., Schalles, J., Binding, C., Cao, Z., Ma, R., Alikas, K., Kangro, K., Gurlin, D., Hà, N., 2020. Seamless retrievals of chlorophyll-a from Sentinel-2 (MSI) and Sentinel-3 (OLCI) in Inland and Coastal waters: A machine-learning approach. Remote Sens. Environ. 240, 111604.
Pearlman, J.S., Barry, P.S., Segal, C.C., Shepanski, J., Beiso, D., Carman, S.L., 2003. Hyperion, as pace-based imaging spectrometer. IEEE Trans. Geosci. Remote Sens. 41, 1160–1173.
Pereira Sandoval, M., Urrego, P., Ruiz-Verdú, A., Tenjo, C., Delegido, J., Soria-Perpinyà, X., Vicente, E., Soria, J., Moreno, J., 2019. Calibration and validation of algorithms for the estimation of chlorophyll-a concentration and secchi depth in inland waters with Sentinel-2. Limnetica 38, 471–487.
Purkis, S.J., Riegl, B.M., 2012. Geomorphology and reef building in the SE Gulf. In: Riegl, B.M., Purkis, S.J. (Eds.), Coral Reefs of the Gulf: Adaptation to Climatic Extremes. Springer, ISBN: 978-94-007-3007-6.
Rajendran, S., Hamad, Al Saad, Sadooni, F.N., S., Nasir., H., Govil., 2021. Remote sensing of Inland Sabkha and study of salinity and temporal stability for sustainable development: A case study from the west coast of Qatar. Sci. Total Environ. 782, 146932.
Rakib, F., Ebrahim, M.A.S., Al-Ansari, ., Husrevoglu, O., Al-Maslamani, I., Aboobacker, V.M., Vethamony, P., 2021. Observed variability in physical and biogeochemical parameters in the central Arabian Gulf. Oceanologia 63 (2), 227–237.
Richard, J., Richard, B., Jakub, N., Christopher, N., Min, X., Song, S., Bo, Y., Hongxing, L., Erich, E., Molly, R., et al., 2018. Evaluating the portability of satellite-derived chlorophyll-a algorithms for temperate inland lakes using airborne hyperspectral imagery and dense surface observations. Harmful Algae 76, 35–46.
Riegl, B.M., Purkis, S.J., 2012. Coral reefs of the gulf: Adaptation to climatic extremes in the world's hottest sea. In: Riegl, B., Purkis, S. (Eds.), Coral Reefs of the Gulf. In: Coral Reefs of the World, vol. 3, Springer, Dordrecht, http://dx.doi.org/10.1007/978-94-007-3008-3_1.
Ruddick, K., et al., 2016. New opportunities and challenges for high-resolution remote sensing of water colour. In: Proceedings of the Ocean Optics. Victoria, CB, Canada.
Sala, I., Navarro, G., Bolado-Penagos, M., Echevarría, F., García, C.M., 2018. High-chlorophyll-area assessment based on remote sensing observations: The case study of Cape Trafalgar. Remote Sens. 10 (2), 165.
Sala, M.M., Peters, F., Sebastián, M., Cardelús, C., Calvo, E., Marrasé, C., Massana, R., Pelejero, C., Sala-Coromina, J., Vaqué, D., Gasol, J.M., 2022. COVID-19 lockdown moderately increased oligotrophy at a marine coastal site. Sci. Total Environ. 812, 151443.
Salem, S.I., Strand, M.H., Higa, H., Kim, H., Kazuhiro, K., Oki, K., Oki, T., 2017. Evaluation of MERIS chlorophyll-a retrieval processors in a complex turbid lake kasumigaura over a 10-year mission. Remote Sens. 9, 1022.
Seim, H., Blanton, J., Elston, S., 2006. Tidal circulation and energy dissipation in a shallow, sinuous estuary. Ocean Dyn. 56, 360–375.
Shafeeque, M., Shah, P., Platt, T., Sathyendranath, S., Menon, N.N., Balchand, A.N., George, G., 2019. Effect of precipitation on chlorophyll-a in an Upwelling Dominated Region along the West Coast of India. J. Coast. Res. 86, 218–224.
Shah, P., Sajeev, R., Thara, K.J., George, G., Shafeeque, M., Akash, S., Platt, T., 2019. A holistic approach to upwelling and downwelling along the South-West Coast of India. Mar. Geodesy 42 (1), 64–84.
Shahzad, M.I., Meraj, M., Nazeer, M., Zia, I., Inam, A., Mehmood, K., Zafar, H., 2018. Empirical estimation of suspended solids concentration in the Indus Delta region using Landsat-7 ETM+ imagery. J. Environ. Manage. 209, 254–261.
Sheppard, C.R., 1993. Physical environment of the gulf relevant to marine pollution: an overview. Mar. Pollut. Bull. 27, 3–8.
Sheppard, C., Al-Husiani, M., Al-Jamali, F., Al-Yamani, F., Baldwin, R., Bishop, J., Benzoni, F., Dutrieux, E., Dulvy, N.K., Durvasula, S.R.V., Jones, D.A., Loughland, R., Medio, D., Nithya n.d.dan, M., Pilling, G.M., Polikarpov, I., Price, A.R.G., Purkis, S.J., Riegl, B., Saburova, M., Namin, K.S., Taylor, O., Wilson, S., Zainal, K., 2010. The Persian/Arabian Gulf: a young sea in decline. Mar. Pollut. Bull. 60, 13–38.
Solonenko, M.G., Mobley, C.D., 2015. Inherent optical properties of jerlov water types. Appl. Opt. 54, 5392–5401.
Sosa-Ávalos, R., Santamaría-del Ángel, E., Acosta-Chamorro, V., Silva-Iñiguez, L., del Carmen Pelayo-Martínez, G., Quijano-Scheggia, G.I., 2021. Phytoplankton primary production during the cold and warm seasons in Manzanillo and Santiago Bays, Mexico. Estuar. Coast. Shelf Sci. 261, 107569.
Stumpner, E.B., Bergamaschi, B.A., Kraus, T.e.C., Parker, A.E., Wilkerson, F.P., Downing, B.D., Dugdale, R.C., M.c., Murrell, Carpenter, K.D., Orlando, J.L., Kendall, C., 2020. Spatial variability of phytoplankton in a shallow tidal freshwater system reveals complex controls on abundance and community structure. Sci. Total Environ. 700, 1343923.
Su, H., Lu, X., Chen, Z., Zhang, H., Lu, W., Wu, W., 2021. Estimating coastal chlorophyll-a concentration from time series OLCI data based on machine learning. Remote Sens. 13, 576.
Sultan, S.A.R., Elghribi, N.M., 1996. Temperature inversion in the Arabian Gulf and the Gulf of Oman. Contin. Shelf Res. 16, 1521–1544.
Swift, S.A., Bower, A.S., 2003. Formation and circulation of dense water in the Persian/Arabian Gulf. J. Geophys. Res. 108 (4(1-15)).
Tang, X., Li, R., Han, D., Scholz, M., 2020. Response of Eutrophication development to variations in nutrients and hydrological regime: A case study in the Changjiang River (Yangtze) Basin. Water 12 (6), 1634.
Toming, K., Kutser, T., Laas, A., Sepp, M., Paavel, B., Nõges, T., 2016. First experiences in mapping lake water quality parameters with Sentinel-2 MSI imagery. Remote Sens. 8, 640.
Tuuli, S., Kristi, U., Dainis, J., Agris, B., Matiss, Z., Tiit, K., 2020. Validation and comparison of water quality products in Baltic Lakes using sentinel-2 MSI and sentinel-3 OLCI data. Sensors 20, 742.
Tzortziou, M., Subramaniam, A., Herman, J.R., Gallegos, C.L., Neale, P.J., Harding, L.W., 2007. Remote sensing reflectance and inherent optical properties in the Mid Chesapeake Bay. Estuar. Coast. Shelf Sci. 72, 16–32.
Vaughan, G.O., Burt, J.A., 2016. The changing dynamics of coral reef science in Arabia. Mar. Pollut. Bull. 105, 441–458.
Wang, X., Gong, Z., Pu, R., 2018. Estimation of chlorophyll-a content in inland turbidity waters using WorldView-2 imagery: a case study of the Guanting Reservoir, Beijing, China. Environ. Monit. Assess. 190, 620.
Wang, Y., Tian, X., Gao, Z., 2021. Evolution of satellite derived chlorophyll-a trends in the Bohai and Yellow Seas during 2002–2018: Comparison between linear and nonlinear trends. Estuar. Coast. Shelf Sci. 259, 107449.
Watanabe, F., Alcantara, E., Rodrigues, T., Rotta, L., Bernardo, N., Imai, N., 2018. Remote sensing of the chlorophyll-a based on OLI/Landsat-8 and MSI/Sentinel-2A (Barra Bonita reservoir, Brazil). Ann. Acad. Bras. Ciênc. 90, 1987–2000.
Xu, M., Liu, H., Beck, R., Lekki, J., Yang, B., Shu, S., Kang, E.L., Anderson, R., Johansen, R., Emery, E., Reif, M., Benko, T., 2019. A spectral space partition guided ensemble method for retrieving chlorophyll-a concentration in inland waters from Sentinel-2A satellite imagery. J. Gt. Lakes Res. 45 (3), 454–465.
Xu, W., Wang, G., Cheng, X., Jiang, L., Zhou, W., Cao, W., 2022. Characteristics of subsurface chlorophyll maxima during the boreal summer in the South China sea with respect to environmental properties. Sci. Total Environ. 820, 153243.
Yacobi, Y.Z., Gitelson, A.A., Mayo, M., 1995. Remote sensing of chlorophyll in Lake Kinneret using high spectral resolution radiometer and Landsat TM: Spectral features of reflectance and algorithm development. J. Plankton. Res. 17 (11), 2155–2173.
Zhang, Y., Ma, R., Duan, H., Loiselle, S., Xu, J., 2014. A spectral decomposition algorithm for estimating chlorophyll-a concentrations in Lake Taihu, China. Remote Sens. 6, 5090–5106.
Zhang, Y., Qin, B., Chen, W., Gao, G., Chen, Y., 2004. Chlorophyll a content and primary productivity of phytoplankton in Meiliang Bay of Taihu Lake. Ying Yong Sheng Tai Xue Bao 15 (11), 2127–2131, Chinese. PMID: 15707327.
Zhao, D.Z., Xing, X.G., Liu, Y.G., Yang, J.H., Wang, L., 2010. The relation of chlorophyll-a concentration with the reflectance peak near 700 nm in algae-dominated waters and sensitivity of fluorescence algorithms for detecting algal bloom. Int. J. Remote Sens. 31, 39–48.
Zheng, G., Di Giacomo, P.M., 2017. Remote sensing of chlorophyll-a in coastal waters based on the light absorption coefficient of phytoplankton. Remote Sens. Environ. 201, 331–341.